Technology

Molecular Cell

# Visualizing Dynamics of Cell Signaling *In Vivo* with a Phase Separation-Based Kinase Reporter

## Graphical Abstract

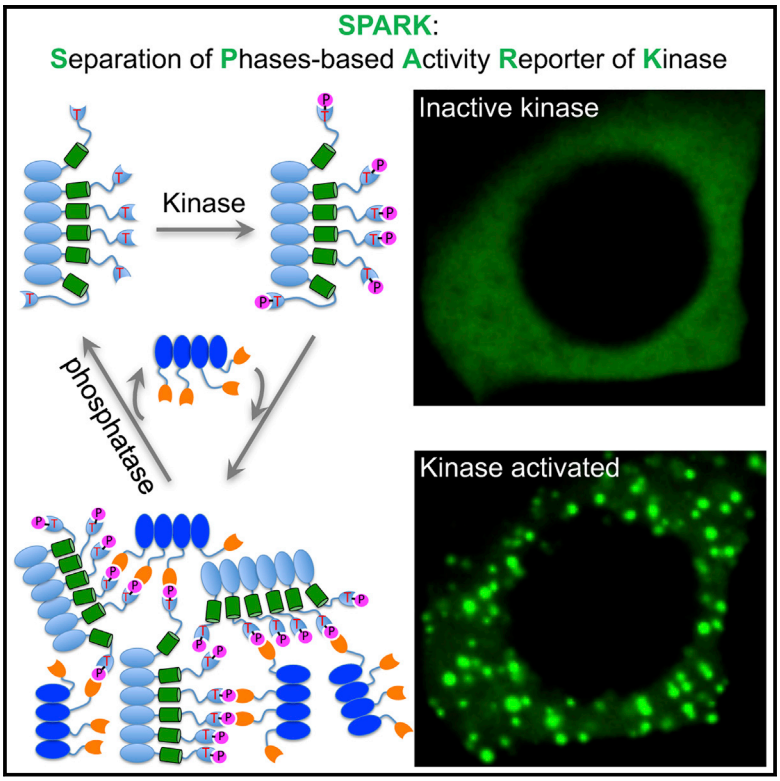


## Highlights

- Rapamycin-inducible protein phase transition is developed
- The kinase reporter SPARK achieves intensive brightness and simple signal pattern
- SPARK reveals dynamic ERK signaling during tissue homeostasis *in vivo*
- SPARK technology enables modular design of other kinases' reporters

## Authors

Qiang Zhang, Hai Huang, Qing Lu, ..., Shaun R. Coughlin, Thomas B. Kornberg, Xiaokun Shu

## Correspondence

xiaokun.shu@ucsf.edu

## In Brief

A separation of phases-based activity reporter of kinase, dubbed SPARK, is designed via multivalent protein-protein interactions utilizing homo-oligomeric coiled coils. The intensive brightness and simple signal pattern of SPARK allow robust and direct visualization of kinase signaling in living animals.

Zhang et al., 2018, Molecular Cell *69*, 1–13
January 18, 2018 Published by Elsevier Inc.
https://doi.org/10.1016/j.molcel.2017.12.008

CellPress

Please cite this article in press as: Zhang et al., Visualizing Dynamics of Cell Signaling *In Vivo* with a Phase Separation-Based Kinase Reporter, Molecular Cell (2017), https://doi.org/10.1016/j.molcel.2017.12.008

Molecular Cell
Technology

# Visualizing Dynamics of Cell Signaling *In Vivo* with a Phase Separation-Based Kinase Reporter

Qiang Zhang,[1,2,4] Hai Huang,[2,4] Qing Lu,[2] Roland Wu,[2] Chan-I Chung,[1,2] Shao-Qing Zhang,[2] Joaquim Torra,[1,2,3] Antonino Schepis,[2] Shaun R. Coughlin,[2] Thomas B. Kornberg,[2] and Xiaokun Shu[1,2,5,*]
[1]Department of Pharmaceutical Chemistry
[2]Cardiovascular Research Institute
University of California, San Francisco, San Francisco, CA 94143, USA
[3]Institut Químic de Sarrià, Universitat Ramon Llull, Via Augusta 390, 08017 Barcelona, Spain
[4]These authors contributed equally
[5]Lead Contact
*Correspondence: xiaokun.shu@ucsf.edu
https://doi.org/10.1016/j.molcel.2017.12.008

## SUMMARY

**Visualizing dynamics of kinase activity in living animals is essential for mechanistic understanding of cell and developmental biology. We describe GFP-based kinase reporters that phase-separate upon kinase activation via multivalent protein-protein interactions, forming intensively fluorescent droplets. Called SPARK (*s*eparation of *p*hases-based *a*ctivity *r*eporter of *k*inase), these reporters have large dynamic range (fluorescence change), high brightness, fast kinetics, and are reversible. The SPARK-based protein kinase A (PKA) reporter reveals oscillatory dynamics of PKA activities upon G protein-coupled receptor activation. The SPARK-based extracellular signal-regulated kinase (ERK) reporter unveils transient dynamics of ERK activity during tracheal metamorphosis in live *Drosophila*. Because of intensive brightness and simple signal pattern, SPARKs allow easy examination of kinase signaling in living animals in a qualitative way. The modular design of SPARK will facilitate development of reporters of other kinases.**

## INTRODUCTION

Temporal dynamics of signaling can elicit distinct cellular responses (Doupé and Perrimon, 2014; Hynes et al., 2013; Lemmon and Schlessinger, 2010; Purvis and Lahav, 2013), and available evidence shows that, even in the same cell type, different dynamics of the same signaling pathway can produce different outcomes (Marshall, 1995; Santos et al., 2007; Sasagawa et al., 2005; Toettcher et al., 2013). Protein kinases mediate cell signaling in animals, and protein phosphorylation is an essential type of post-translational modification involved in signal transduction (Hunter, 2009; Manning et al., 2002; Pawson and Scott, 2005). Therefore, a mechanistic understanding of animal development and tissue biology will benefit from visualizing dynamics of kinase activity in physiological contexts (Doupé and Perrimon, 2014; Hynes et al., 2013; Sopko and Perrimon, 2013). For example, extracellular signal-regulated kinase (ERK) is highly conserved from single-celled organisms to multicellular animals, and many receptor tyrosine kinases (RTKs) that play central roles in regulating animal development converge on the common ERK pathway (Sopko and Perrimon, 2013). Differential dynamics of ERK signaling is believed to be one of the mechanisms that discriminates different RTKs (Hynes et al., 2013; Purvis and Lahav, 2013; Shilo, 2014; Sopko and Perrimon, 2013; Toettcher et al., 2013).

To visualize dynamic kinase signaling in living cells and animals, genetically encoded fluorescent reporters are ideal because they allow non-invasive dynamic imaging. Examples include the kinase reporters that are based on fluorescence resonance energy transfer (FRET) between variants of the GFP, e.g., a cyan and a yellow fluorescent protein derived from the GFP (Miyawaki and Niino, 2015; Oldach and Zhang, 2014; Rodriguez et al., 2017; Sanford and Palmer, 2017). These FRET reporters are valuable tools for imaging kinase signaling in living cells, including protein kinase A (PKA) (Zhang et al., 2001, 2005) and ERK (Harvey et al., 2008). While FRET reporters achieve subcellular resolution and have recently unveiled compartmentalized kinase signaling in cultured single cells (Mo et al., 2017), *in vivo* use of the FRET reporters is problematic because of their small fluorescence ratio change of acceptor over donor fluorophores (Kardash et al., 2011). Thus, a robust fluorescent reporter for imaging dynamic kinase activity in living animals is much needed. Such a reporter should have large signal-to-noise ratio and fast kinetics in order to detect when and in which tissues and cells a kinase is activated during development and other *in vivo* settings.

Another example of genetically encoded kinase reporters is the phosphorylation-dependent GFP translocation-based kinase reporters, which shuttle between cytoplasm and nucleus of cultured cells upon kinase activation (Regot et al., 2014). Most of these reporters achieve large fluorescence ratio change between cytoplasm and nucleus compared to FRET reporters. For instance, the ERK reporter has 2- to 3-fold fluorescence ratio change upon ERK activation. The PKA reporter (PKA-KTR), in contrast, only achieves ~30% ratio change upon PKA activation

(Regot et al., 2014). Robust detection of kinase activity in living animals may require larger dynamic range (fluorescence change) and simpler signal pattern, because *in vivo* imaging is known to be challenging due to tissue autofluorescence and light scattering, rapid cell movement, and shape changes (Kardash et al., 2011).

## DESIGN

Since biological performance of kinase reporters is determined by their physical or chemical principles, to overcome the challenges for *in vivo* imaging, we seek to design and demonstrate phase separation-based kinase reporters. The rationale is that fluorescence change of a kinase reporter is determined by kinase activity-dependent changes to the brightness of a digital fluorescence image, which not only depends on intrinsic brightness (= quantum yield × extinction coefficient) of the fluorophore but also is proportional to the number of imaged fluorophores per pixel (Waters, 2009). FRET kinase reporters report changes of intrinsic brightness of donor and/or acceptor fluorophores via FRET (Fairclough and Cantor, 1978). A different approach is to design reporters that change the number of imaged fluorophores per pixel. We thus decided to design a different class of fluorescent reporters that, upon kinase activation, phase-separate and form highly concentrated droplets.

Our design was inspired by a recent work showing that multivalent interactions drive protein phase separation and formation of protein droplets (Li et al., 2012). Therefore, we rationally designed multivalent protein-protein interaction (PPI)-driven phase separation-based kinase reporters; (1) to introduce multivalency, we utilized *de novo* designed homo-oligomeric coiled coils; (2) to sense kinase activity, we introduced kinase activity-dependent PPI—a consensus kinase substrate sequence (a phosphopeptide) and a phosphopeptide-binding domain; and (3) to obtain fluorescence signal, we incorporated EGFP into the reporter. We chose EGFP as the fluorophore because its fluorescence requires no cofactor except molecular oxygen and because its use in living cells and animals has been validated in many contexts (Tsien, 1998, 2009).

The phase separation-based kinase reporter is called SPARK (separation of phases-based activity reporter of kinase). Upon kinase activation, the kinase substrate peptide is phosphorylated and then interacts with phosphopeptide-binding domain; the resulting multivalent PPI leads to highly concentrated (10×) EGFP droplets. The intensive brightness and punctal signal pattern enable SPARK to robustly detect kinase activity *in vivo*. SPARK has ~20-s response time and is reversible, with no perturbation of kinase signaling and no apparent toxicity in transgenic animals. The modular design of SPARK allows straightforward design of reporters of other kinases by swapping the kinase substrate sequence and the phosphopeptide-binding domain.

## RESULTS AND DISCUSSION

### Design of Rapamycin-Inducible Protein Phase Separation

To develop phase separation-based kinase reporters, we first sought to design a general platform for inducible protein phase separation via multivalent PPI. We chose the well-characterized FKBP and Frb as an inducible PPI system since their interaction can be robustly induced by rapamycin (Banaszynski et al., 2005). To design multivalent reporters, it is not ideal to use multiple repeat protein domains, which not only will make the reporter protein extremely large but also may be problematic for making transgenic animals (e.g., potential DNA recombination). Thus, instead of using multiple repeats, we turned to *de novo*-designed homo-oligomeric coiled coils. We named these coiled coils as HO-Tag (homo-oligomeric tag). Most *de novo*-designed coiled coils are short peptides, ~30 amino acids (Woolfson et al., 2015), and are, therefore, ideal tags to introduce multivalency. We chose seven coiled coils previously characterized in protein *de novo* design studies (Grigoryan et al., 2011; Huang et al., 2014; Thomson et al., 2014). These coiled coils are here named from HOTag1 to HOTag7 (Figure S1A). To achieve high multivalency, we chose coiled coils that have high stoichiometry, forming tetramer, pentamer, hexamer, and heptamer.

Characterization of these HOTags using the FKBP and Frb PPI pair in HEK293 cells showed that HOTag3 and HOTag6 were most robust in driving rapamycin-inducible protein droplet formation over a wide range of protein concentrations (see the Star Methods and Figures S1A–S1D, S2, and S3). HOTag3 and HOTag6 were highly soluble when fused to FKBP and EGFP fusion (Figures 1A and 1B). To examine kinetics of the EGFP phase separation upon rapamycin-induced PPI in living cells, we conducted time-lapse fluorescence imaging, which revealed that fluorescent droplets formed within 2 min upon rapamycin addition (Figure 1C; Movie S1). Since this includes the time necessary for the rapamycin to diffuse through the cell membrane, the kinetics of droplet formation are expected to be faster (see below). The fluorescent droplets could be qualitatively and easily identified because of their brightness and signal pattern. They could also be quantified and plotted as a fluorescent histogram at pixel level, which showed high brightness and large signal (Figure 1C). Since the hexameric HOTag3 and the tetrameric HOTag6 (Figure S1E) can robustly drive protein phase separation upon protein interaction, we chose HOTag3/6 as the pair for use in kinase reporters.

Protein phase separation and formation of droplets can be attributed to two main factors: PPI and multivalency (Banani et al., 2017; Hyman et al., 2014; Li et al., 2012). In our system, rapamycin induced PPI between FKBP and Frb whereas multivalency was introduced by the HOTags. Rapamycin and HOTags induced multivalent PPIs that drove protein phase separation and formation of EGFP droplets (Figure 1D, EGFP is not shown); the addition of rapamycin induced protein separation into two phases: a dilute phase and a concentrated phase. The high-concentration phase was the protein condensate or droplet (Figure 1D). At equilibrium state, the chemical potential of the dilute and condensed phases were equivalent for both proteins and solvent. Our findings show that the paired HOTag3 and HOTag6 are excellent multivalent tags capable of driving protein phase separation upon PPI over a large range of protein concentrations. We suggest that this HOTag pair will be a valuable tool for many applications, including the induction of protein phase separation for biological investigation of function and for

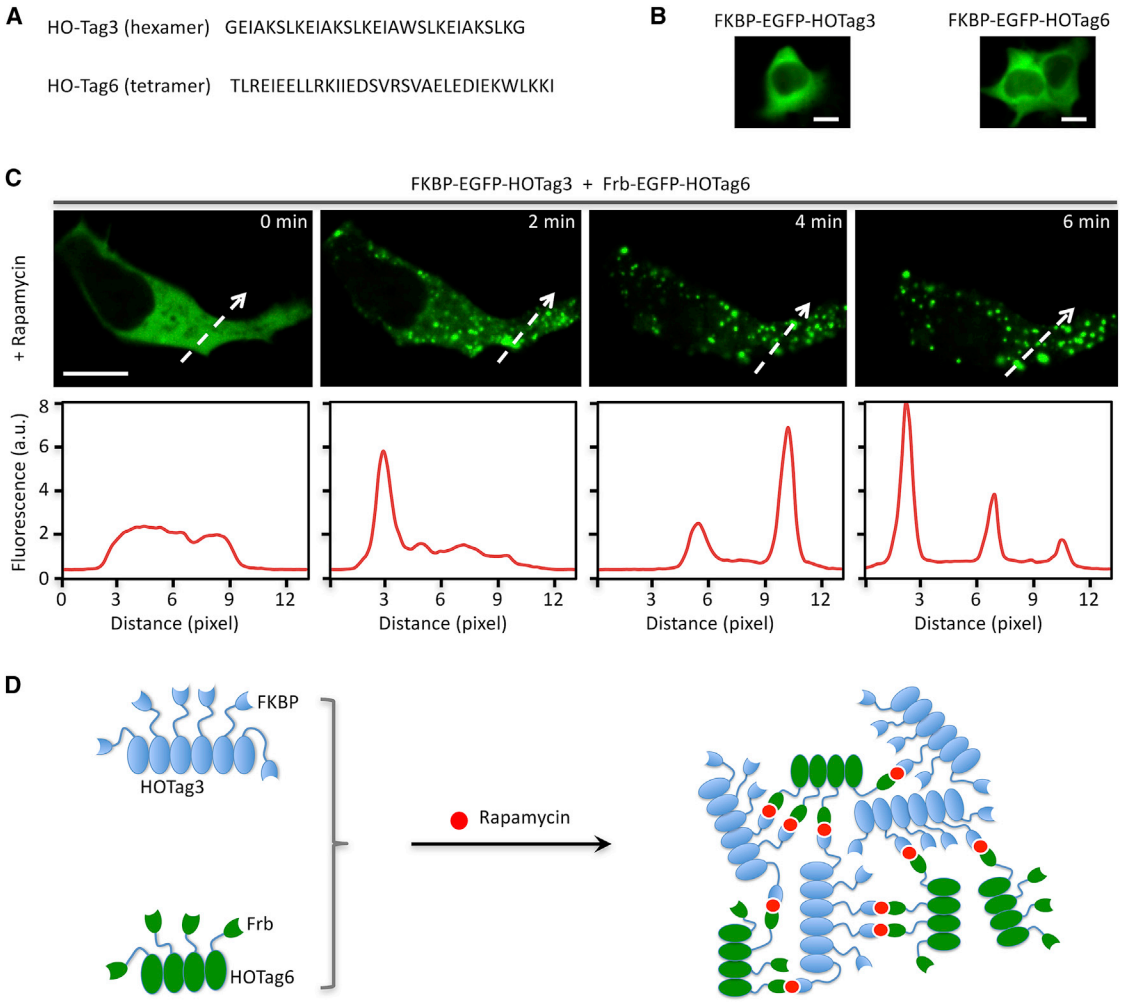


**Figure 1. Rational Design of Inducible Protein Phase Separation by Protein-Protein Interaction**

(A) *De novo*-designed coiled coils are used as homo-oligomeric tag (HOTag), which introduces multivalency.

(B) HOTags fused to EGFP and FKBP were expressed in HEK293 cells.

(C) Time-lapse images of cells expressing HOTag fusions upon the addition of rapamycin. FKBP-EGFP-HOTag3 and Frb-EGFP-HOTag6 were co-transfected. Histograms are shown corresponding to the dashed line in the fluorescence images.

(D) Schematic diagram of induced protein phase separation with HOTags. Left: FKBP-EGFP (not shown)-HOTag3 hexamer and Frb-EGFP (not shown)-HOTag6 tetramer are shown. Right: protein condensate or droplet is shown.

Scale bar, 10 μm.

characterizing the consequences of protein phase separation (Banani et al., 2017).

## Design of Phase Separation-Based Activity Reporter of Protein Kinase A

To determine whether HOTag3 and HOTag6 can be used to design a SPARK, we generated a construct for detecting PKA activity. PKA is an important mediator of G protein-coupled receptor (GPCR) signaling (Taylor et al., 2012), but the signal of current PKA reporters, including both FRET- and translocation-based reporters, is small, with ~30% ratio change of the fluorescence (Regot et al., 2014; Zhang et al., 2005).

To design a SPARK-based PKA reporter (named PKA-SPARK), we utilized a consensus peptide sequence that is specifically phosphorylated by PKA (Durocher et al., 2000). To introduce PKA activity-dependent PPI, we chose forkhead-associated domain 1 (FHA1), which is a phosphothreonine-binding domain (Durocher et al., 2000). Both motifs have been successfully used in the FRET-based PKA reporters (Zhang et al., 2005). We fused the PKA substrate sequence to EGFP followed by HOTag3, and we fused FHA1 to HOTag6. These two fusion sequences were connected by a self-cleaving 2A sequence (Figure 2A). The rationale is that substrate and the FHA1 induce PKA activity-dependent PPI, and the two HOTags introduce multivalency; upon PKA activation, multivalent PPIs are induced, leading to phase separation and formation of EGFP droplets (Figure 2A).

To test this construct, we added the β-adrenergic agonist isoprenaline to HEK293 cells that endogenously express

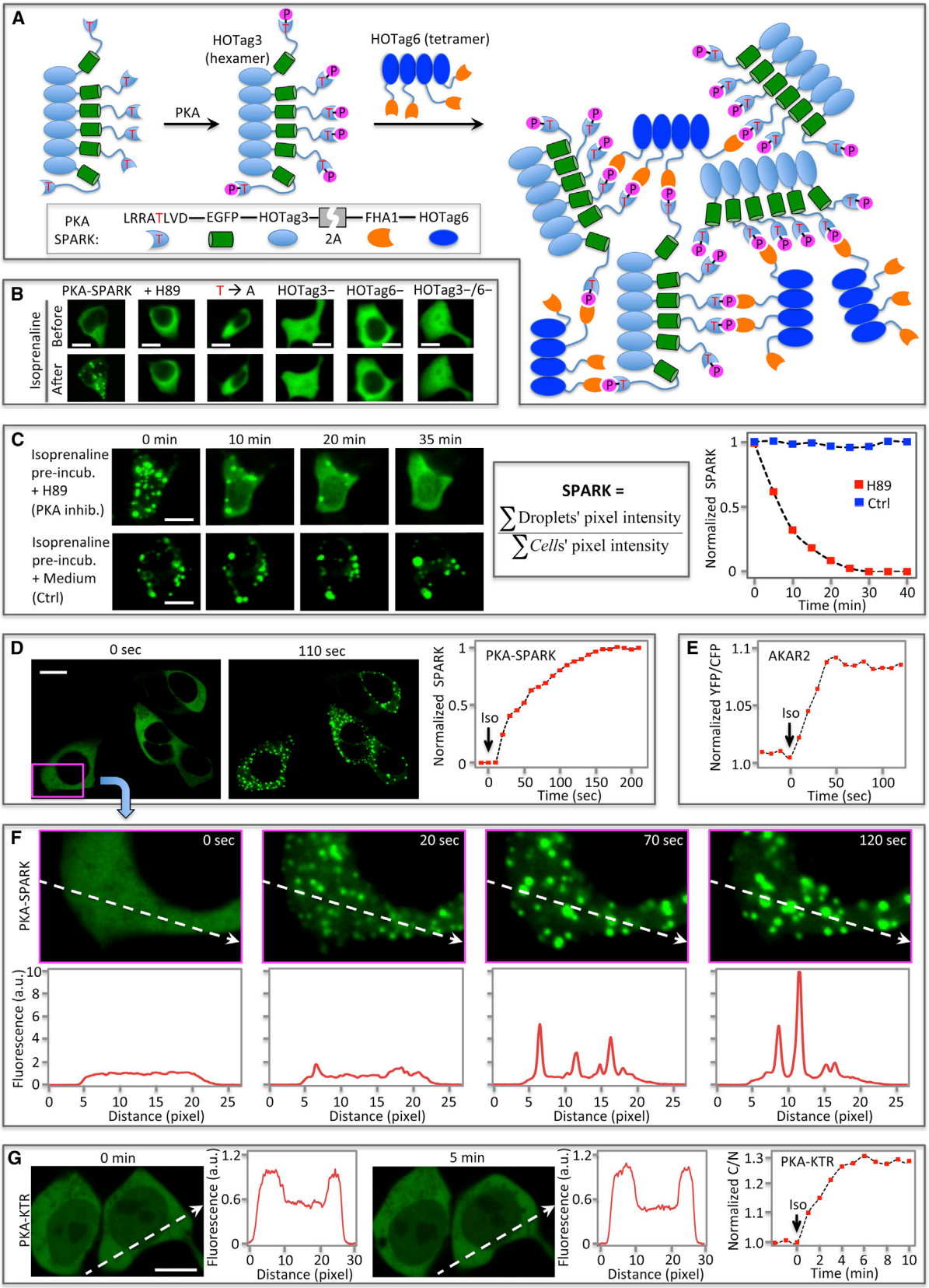


*(legend on next page)*

β-adrenergic receptors (βARs). βAR activation induces guanosine diphosphate (GDP) for guanosine triphosphate (GTP) exchange in the heterotrimeric G protein Gs, and GTP-bound Gαs activates adenylyl cyclase (AC), which converts ATP into cyclic AMP (cAMP) that activates PKA. Upon the addition of the βAR agonist, fluorescent droplets formed in the reporter-expressing HEK293 cells (Figure 2B). In contrast, pre-incubation with the PKA inhibitor H89 abolished isoprenaline-induced droplet formation (Figure 2B). These results suggest that PKA activation induced EGFP phase separation. To confirm that the phase separation results from phosphorylation of PKA-SPARK at the expected threonine residue, we changed the threonine to alanine in the PKA substrate sequence (LRRATLVD). This mutant PKA-SPARK did not form fluorescent droplets in cells stimulated with isoprenaline. These results suggest that phosphorylation of the single threonine is responsible for the PKA activity-dependent phase separation of the reporter. Lastly, removal of either HOTag3 or HOTag6 or both abolished droplet formation upon isoprenaline stimulation, indicating that both HOTags are required for droplet formation. Our data thus suggest that PKA activity-triggered multivalent interaction between FHA1-HOTag6 and the PKA substrate peptide-EGFP-HOTag3 leads to EGFP phase separation.

We next asked whether phase separation of the reporter is reversible, i.e., whether the EGFP droplets disassemble or dissolve when PKA is inactivated. We pre-incubated cells with isoprenaline to induce phase separation, then removed isoprenaline and added H89 to inactivate PKA. The EGFP droplets disassembled rapidly (Figure 2C), which is consistent with studies that used a FRET PKA reporter (AKAR2) and reported that H89 inactivates isoprenaline-induced PKA activation (Zhang et al., 2005). As a control, the EGFP droplets were stable over time in the cells with removal of isoprenaline but addition of medium without H89 (Figure 2C). The reversibility of the EGFP droplets suggests that the droplets are accessible to protein phosphatases, which is consistent with previous studies that protein droplets not only contain scaffold proteins responsible for droplet formation but also contain client proteins, which interact with scaffold proteins but are not required for the droplet formation (Banani et al., 2016, 2017). To examine whether PKA-SPARK could quantitatively measure the droplets' disassembly over time after PKA inhibition, we defined SPARK signal as the sum of fluorescent droplets' pixel intensity divided by sum of cells' pixel intensity (Figure 2C). Upon the addition of H89, the SPARK signal decreased over time. In contrast, for the control the SPARK signal remained constant over time (Figure 2C). These results suggest that SPARK signal quantitatively described droplets' disassembly upon PKA inhibition.

We also conducted time-lapse fluorescence imaging of PKA-SPARK at 10 s/frame. Fluorescent droplets formed after the addition of isoprenaline, and the SPARK signal increased over time (Figure 2D). PKA activation upon the addition of isoprenaline was confirmed by AKAR2 (Figure 2E). We detected small droplets of PKA-SPARK as early as at 20 s upon the addition of isoprenaline (Figure 2F). The quick activation of PKA is consistent with rapid activation of the βAR-cAMP-PKA pathway. The small droplets grew quickly and coalesced into large and intensively fluorescent droplets, which were up to 10-fold brighter than the cellular fluorescence before PKA activation (Figure 2F). In contrast, PKA-KTR showed much smaller fluorescence change (Figure 2G). Therefore, PKA-SPARK achieved up to a 10-fold fluorescence increase, which was advantageous to AKAR2 and PKA-KTR, which had ~10% (Figure 2E) and ~30% (Figure 2G) fluorescence ratio change, respectively. Our results demonstrate that PKA-SPARK achieves a large dynamic range, high brightness, and fast kinetics for reporting kinase activity. Furthermore, PKA-SPARK could be used with other fluorescent proteins for cellular imaging, such as histone 2B (H2B)-fused monomeric infrared fluorescent protein (mIFP) (Yu et al., 2015) and a red fluorescent protein mCherry (Shaner et al., 2004) in the cells (Figure S4A; Movie S2). We also verified that PKA-SPARK could detect PKA activity over a wide range of reporter expression (Figure S4B). Lastly the concentration of PKA-SPARK (2–10 μM) appeared to have no effect on the kinetics of droplet assembly (Figure S4C) and disassembly (Figure S4D).

**Figure 2. Design and Characterization of Phase Separation-Based Activity Reporter of Protein Kinase A**

(A) Schematic diagram of the reporter. P represents the phosphate group.

(B) Fluorescence images of the HEK293 cells expressing the PKA reporter PKA-SPARK before and after the addition of beta adrenergic agonist isoprenaline. Cells were not pre-incubated with other molecules unless otherwise noted. +H89, the PKA inhibitor H89 was added 5 min before the addition of isoprenaline; T → A, the phosphothreonine in PKA-SPARK was mutated to alanine; HOTag3−, HOTag3 was removed; HOTag6−, HOTag6 was removed; HOTag3−/6−, HOTag3 and HOTag6 were removed.

(C) Time-lapse fluorescence images of cells expressing PKA-SPARK. Cells were pre-incubated with isoprenaline for 5 min. Isoprenaline was then removed. Upper images were taken after the addition of H89. Lower images were taken after the addition of medium solution without H89. Middle: definition of the SPARK signal is given; see details in the STAR Methods. Right: normalized SPARK signal (from the cell shown in the left images) was plotted against time.

(D) Fluorescence images of cells stimulated with isoprenaline. Cells expressed PKA-SPARK. Right: normalized PKA-SPARK signal (averaged from the cells shown on images in the left) was plotted against time.

(E) Time-dependent fluorescence ratio change of AKAR2 upon the addition of isoprenaline in HEK293 cells. The normalized ratio of yellow fluorescence of YFP (yellow fluorescent protein) over cyan fluorescence of CFP (cyan fluorescent protein) was plotted against time.

(F) Time-lapse images of the zoomed-in area shown in (D). Lower row: fluorescence histograms correspond to the dashed lines in the upper images. Note: the dashed line of the 120-s image is in a relatively bright area (the upper-left area is relatively dark), and the sum of the entire cell's fluorescence compared to that at time 0 is within 10%.

(G) Fluorescence images of cells stimulated with isoprenaline. Cells expressed a recently developed PKA reporter PKA-KTR. PKA-KTR is based on GFP translocation between cytoplasm and nucleus upon PKA activation. Fluorescence histograms corresponding to the dashed line in the images are shown next to the fluorescence images. Normalized fluorescence of cytoplasm over nucleus (C/N) was plotted against time.

Scale bars, 10 μm.

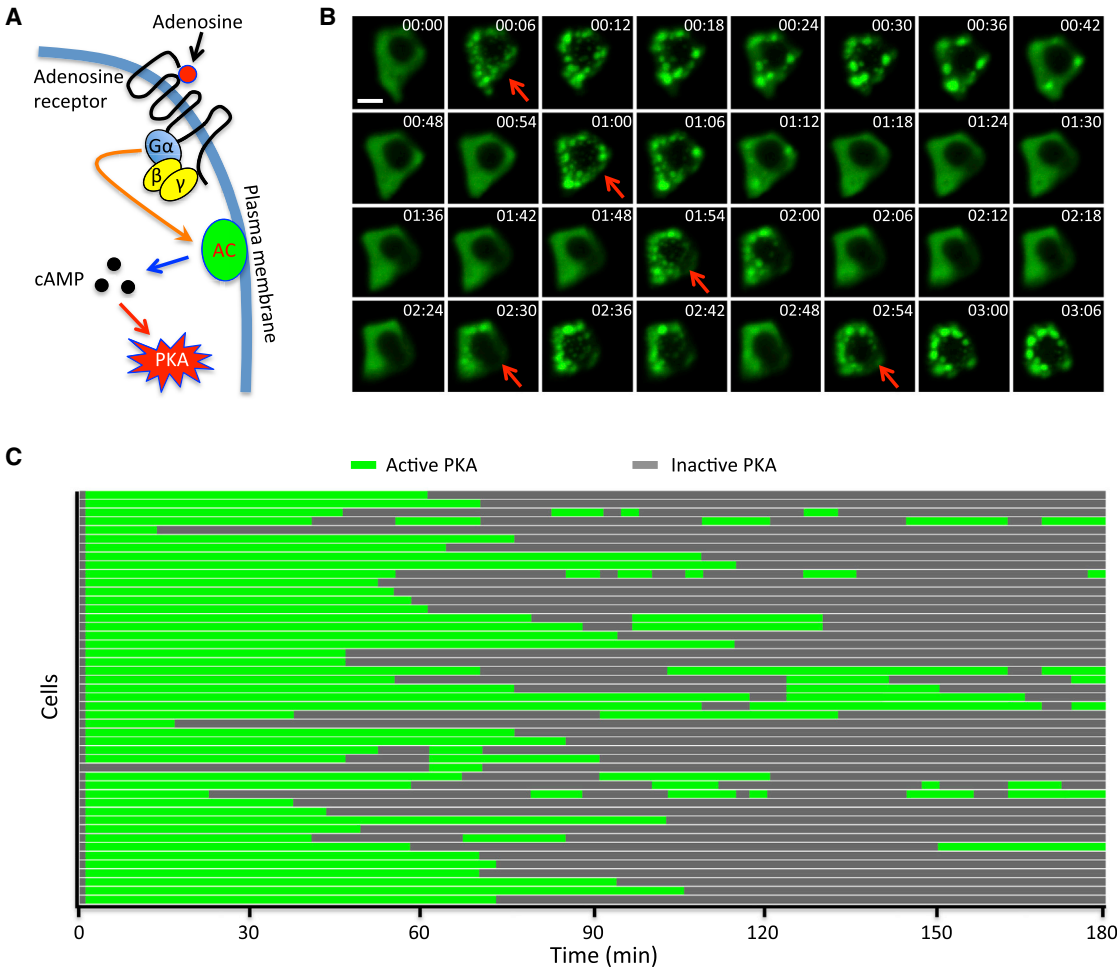


**Figure 3. SPARK Visualizes Dynamic PKA Activity upon Adenosine-Induced GPCR Activation**

(A) Schematic diagram of signaling pathways from the GPCR ligand adenosine to PKA activation. AC, adenylyl cyclase.

(B) Time-lapse fluorescence images upon the addition of adenosine. Images were taken for ~3 hr. Scale bar, 10 μm.

(C) Differential PKA activity in single cells upon the addition of adenosine.

While quantitative analysis can be performed, we emphasize that the advantage of PKA-SPARK is that its intensive fluorescence and simple signal pattern allow easy and straightforward examination of PKA signaling in a qualitative way, based on raw images with no requirement of quantitative data analysis (Movie S3). This is in contrast to the previous PKA reporters, including AKAR2 and PKA-KTR, in which the small fluorescence change makes it difficult to identify PKA activity without quantitative data analysis. Therefore, the SPARK technology represents another class of fluorescent reporters for direct visualization of kinase signaling.

## SPARK Visualizes Dynamic PKA Activity upon GPCR Activation

To determine whether PKA-SPARK could reveal the dynamics of PKA activity, we activated PKA via two types of GPCRs: βARs and adenosine receptors (ARs) (Chen et al., 2013; Higley and Sabatini, 2010; Lebon et al., 2011; Ohta et al., 2006). We added isoprenaline to activate endogenous βARs in HEK293 cells. EGFP droplets formed and persisted for at least 3 hr, suggesting sustained PKA activity (Figure S5; Movie S4). Pre-incubation of cells with the βAR antagonist carvedilol abolished the sustained PKA-SPARK signals induced by isoprenaline (Figure S6; Movie S5).

To activate endogenous ARs in HEK293 cells, we added adenosine, but unlike the prolonged PKA activation via βAR, we detected oscillatory dynamics of PKA-SPARK. Some cells displayed multiple cycles of PKA-SPARK phase separation (Figures 3A and 3B; Movies S6 and S7). The first pulse of PKA-SPARK droplets lasted for about an hour for most cells. Subsequent pulses had relatively short duration, mostly 10–30 min. But shorter (as low as 3 min) and longer (up to 1 hr) periods were also observed (Figure 3B). The AR antagonist caffeine abolished the PKA-SPARK signals (Figure S7; Movie S8) (Fredholm et al., 1999; Jazayeri et al., 2017). While our data unveil interesting oscillatory PKA activities when HEK293 cells are stimulated with adenosine, detailed mechanisms of the oscillatory behavior will require further investigations.

## SPARK Can Be Used to Design an Activity Reporter for ERK

The modular design of SPARK should lend itself to use for other kinases. To determine whether the SPARK design generalizes, we chose the highly conserved kinase ERK, which regulates numerous biological processes during animal development, including cell proliferation, differentiation, and migration (Chen and Krasnow, 2014; Sopko and Perrimon, 2013). To design a SPARK-based ERK reporter (ERK-SPARK), we utilized the ERK activity-sensing motifs that were used for the FRET-based ERK reporters (Harvey et al., 2008; Komatsu et al., 2011). One of the ERK activity-sensing motifs is a phosphopeptide sequence from Cdc25C, followed by an ERK-specific docking site that determines substrate specificity (Lee et al., 2004; Sheridan et al., 2008). The companion fragment is a WW domain that binds the phosphorylated substrate. To construct the ERK-SPARK, we fused the ERK substrate sequence to EGFP followed by HOTag3 and the WW domain to EGFP followed by HOTag6 (Figure 4A). The two fusions were connected by a self-cleaving 2A sequence. The expectation is that substrate motif and the WW domain induce ERK activity-dependent PPI such that, upon ERK activation, the HOTags and the sensing motifs together induce multivalent PPI of the reporters, which then phase-separate and form fluorescent droplets.

To characterize ERK-SPARK, we added epidermal growth factor (EGF) to HEK293 cells. EGF binds the EGF receptor, resulting in ERK activation. As expected, EGFP droplets formed upon the addition of EGF (Figure 4B). In contrast, cells expressing a reporter with a mutated CDC25C peptide fragment with a threonine-to-alanine substitution that was not expected to be phosphorylated by ERK did not exhibit the formation of EGFP droplets after EGF treatment (Figure 4B). Because the ERK-docking site was previously shown to be critical for ERK recognition and binding to substrate (Lee et al., 2004; Sheridan et al., 2008), we also generated a reporter lacking the 4-amino acid-docking site. As expected, this mutated reporter did not show phase separation upon the addition of EGF (Figure 4B). Lastly, removal of either HOTag3 or HOTag6 or both abolished droplet formation upon EGF stimulation, indicating that both HOTags are required for droplet formation.

We also conducted time-lapse imaging and analyzed SPARK signal, which revealed transient ERK activation upon EGF addition (Figure 4C). The level of ERK-SPARK signal was correlated with the level of dually phosphorylated ERK (ppERK) measured by western blot (Figure 4C; Figure S8A), suggesting that ERK-SPARK can quantitatively measure ERK activity level. The transient ERK activation in HEK293 cells upon EGF stimulation was also confirmed by the FRET ERK reporter EKAR (Figure S8B).

To examine specificity of ERK-SPARK, we pre-incubated the cells with the ERK inhibitor PD 0325901, which abolished phase separation of the reporter upon the addition of EGF (Figure 4D). Pre-incubation with inhibitors for other MAPK family kinases, specifically the JNK inhibitor SB 203580 or the p38 inhibitor VIII, did not abolish the formation of EGFP droplets upon EGF addition (Figure 4D). These results suggest that ERK-SPARK specifically reports ERK activity under the conditions used.

Several GPCRs have been reported to activate ERK signaling (DeFea et al., 2000; Lefkowitz and Shenoy, 2005; Luttrell et al., 2001). To investigate whether ERK-SPARK might detect GPCR-induced ERK activity, we added the peptide SFLLRN to HEK293 cells. This hexapeptide is a full agonist for protease-activated receptor-1 (PAR1) (Coughlin, 2000; Vu et al., 1991a, 1991b). Time-lapse imaging revealed abundant EGFP droplets upon addition of the agonist; the signal peaked at around 6–9 min and dissolved between 15 and 20 min (Figure 4E; Movie S9). These results suggest that ERK-SPARK detects ERK activity via endogenous PAR1 in HEK293 cells. Furthermore, the PAR1-induced ERK activity appears to be transient, lasting about 10 min. Therefore, ERK-SPARK will be a useful tool for imaging ERK signaling that is activated via various pathways, including RTKs and GPCRs.

## SPARK Reports ERK Activity in Animal Tissues without Perturbing Signaling or Development

As FRET-based kinase reporters are problematic for animal imaging due to their weak signal, we decided to determine whether the SPARK-based kinase reporters are applicable to animal imaging. First, we created an ERK-SPARK transgenic line of *Drosophila*, and we expressed the reporter in the air sac primordium (ASP) of the *Drosophila* tracheal system. In the ASP, fibroblast growth factor (FGF) is an essential mitogen and FGF receptor (FGFR)-induced ERK signaling has been well established (Sato and Kornberg, 2002; Shilo, 2014). Indeed, we detected EGFP droplets in the ASP (Figure 5A). To confirm that the observed EGFP droplets resulted from a phosphorylation event, we expressed an ERK-unresponsive mutant of the reporter in which the threonine was changed to alanine. Although cells in the ASP had green fluorescence, no EGFP droplets were detected, suggesting that formation of the EGFP droplets in the ASP is dependent on ERK phosphorylation of the reporter.

Next, we expressed a dominant-negative form of FGFR ($FGFR^{DN}$) in the trachea (Reichman-Fried and Shilo, 1995); it abolished EGFP droplets. In contrast, with a brief pulse of elevated expression of FGF (via heat shock in an animal fly carrying an HS-FGF transgene) (Sato and Kornberg, 2002), the ERK-SPARK signal became more abundant and the EGFP droplets appeared throughout the organ. These data thus suggest that the observed ERK activation is induced by FGF signaling, consistent with previous studies (Sato and Kornberg, 2002).

Second, we expressed ERK-SPARK in the *Drosophila* wing imaginal disc, a tissue that requires epidermal growth factor receptor (EGFR)-dependent signaling (Sturtevant et al., 1994; Gabay et al., 1997). To examine ERK-SPARK in this tissue, we expressed both ERK-SPARK and the ERK-unresponsive mutant (T → A mutation). The imaginal disc that expressed ERK-SPARK had abundant fluorescent droplets (Figure 5B; Movie S10). In contrast, discs that expressed the mutant ERK-SPARK had no droplets. Most of the fluorescent droplets were at the dorsoventral boundary and distal hinge of the wing pouch, a pattern that overlaps with the regions that stain with antibody directed against doubly phosphorylated ERK (dpERK) (Gabay et al., 1997). To determine whether expression of the reporter ERK-SPARK perturbed ERK signaling, we first

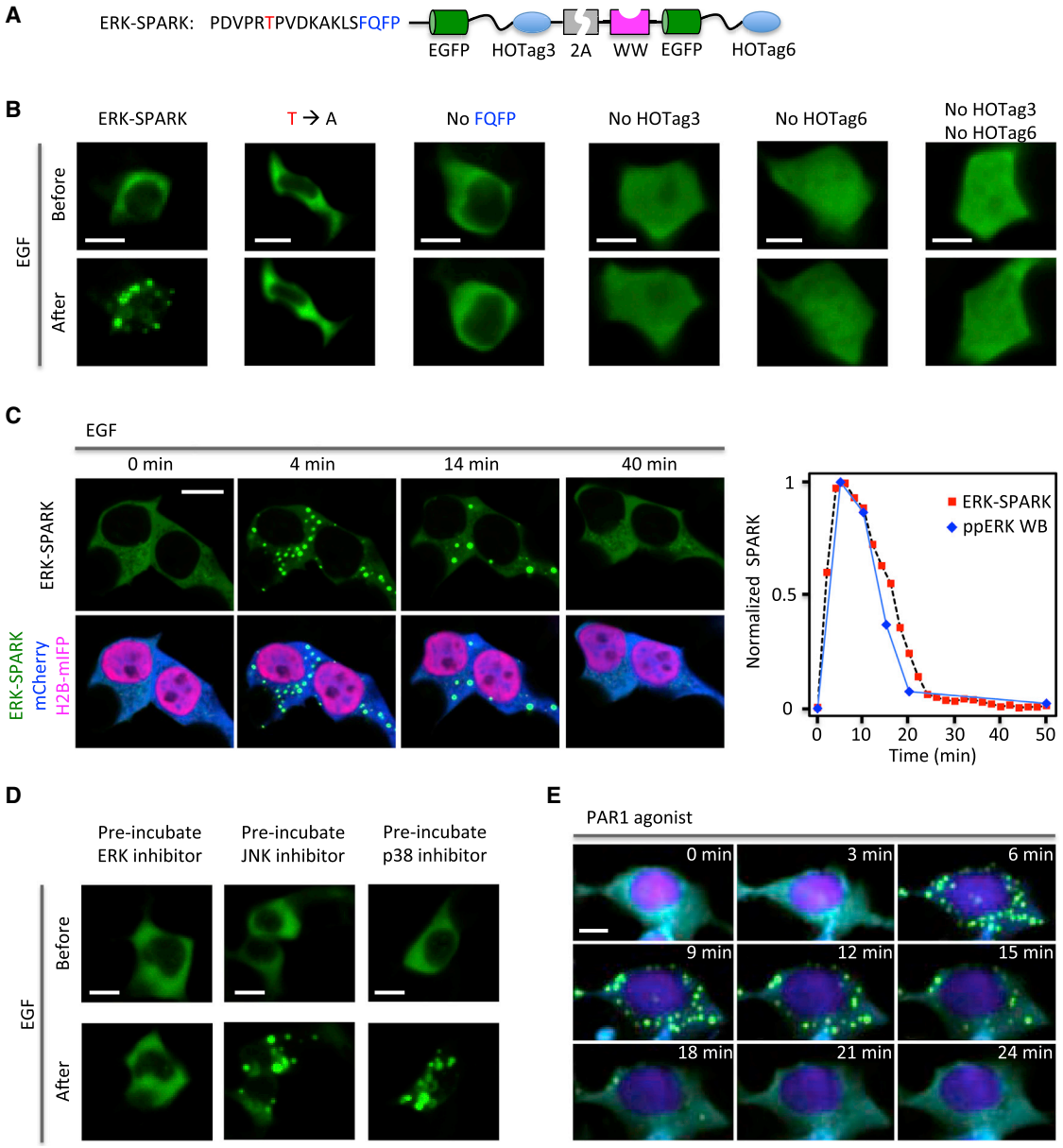


**Figure 4. Design and Characterization of Phase Separation-Based Activity Reporter of ERK**

(A) Schematic diagram of the phase separation-based ERK reporter ERK-SPARK. 2A is a self-cleaving peptide. The phosphothreonine is shown in red. P represents the phosphate group.

(B) Fluorescence images of HEK293 cells expressing ERK-SPARK and its mutant forms before and after the addition of the growth factor EGF. T → A, the phosphothreonine was mutated to alanine; no FQFP, the docking site FQFP was deleted; no HOTag3, HOTag3 was deleted; no HOTag6, HOTag6 was deleted; no HOTag3/no HOTag6, HOTag3 and HOTag6 were both deleted.

(C) Time-lapse fluorescence images of cells expressing ERK-SPARK upon the addition of EGF. Right: normalized SPARK signal (averaged from cells in the left images) was plotted against time; normalized western blot of ppERK was also plotted against time.

(D) Fluorescence images of HEK293 cells expressing ERK-SPARK upon the addition of EGF. The cells were incubated with various inhibitors (left, ERK inhibitor PD 0325901; middle, JNK inhibitor VIII; and right, p38 inhibitor SB 203580).

(E) Time-lapse images of cells expressing ERK-SPARK upon the addition of PAR1 agonist.

In (C) and (E), cells expressing ERK-SPARK were also labeled with mCherry and a nucleus-located monomeric infrared fluorescent protein (mIFP) fused to histone 2B (H2B).

Scale bar, 10 μm (B–E).

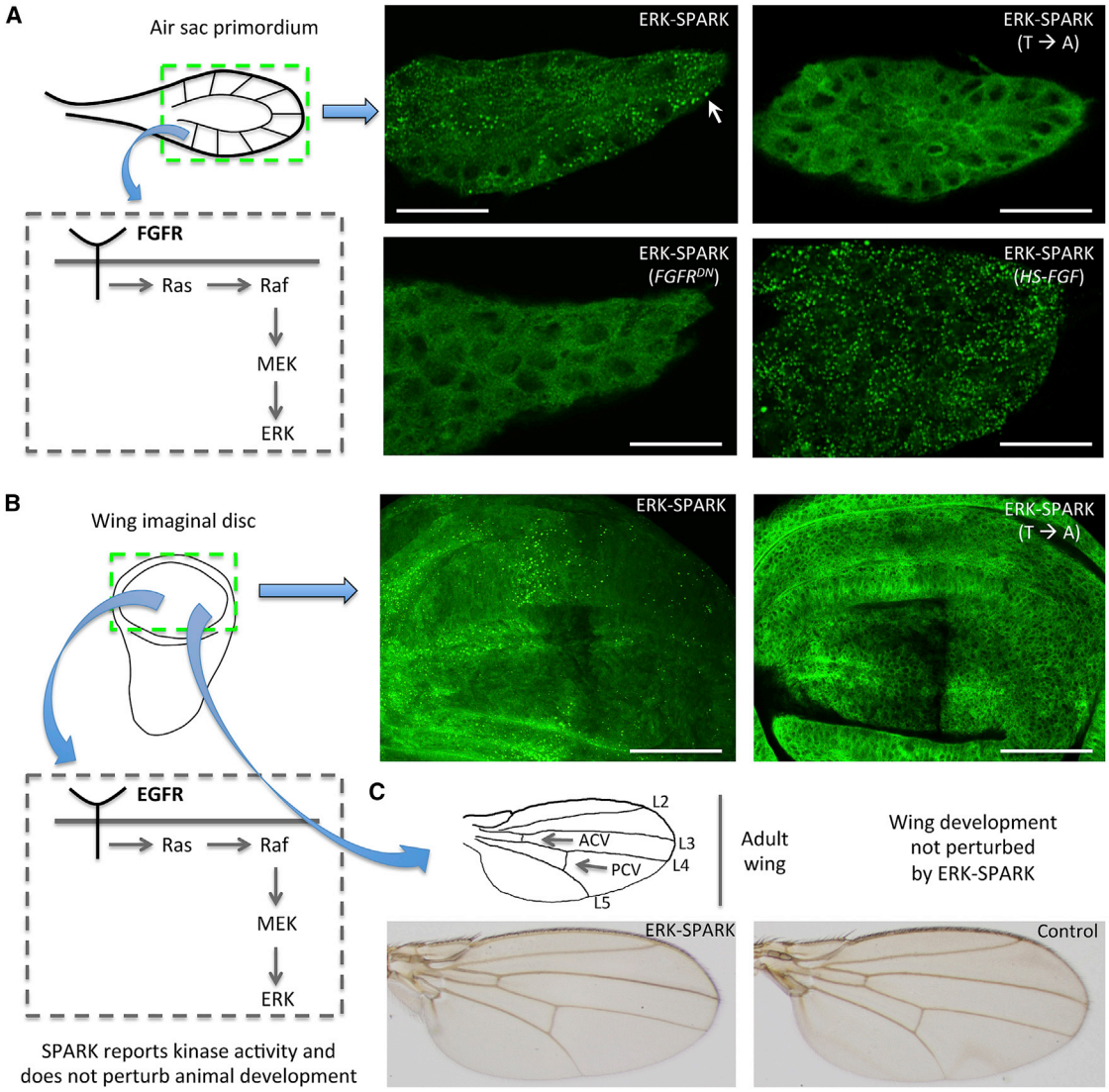


**Figure 5. SPARK Reports ERK Activity in *Drosophila* Tissues without Perturbing Animal Development**

(A) Left: schematic diagrams of the air sac primordium (ASP) and the FGFR/ERK-signaling pathway. Right: fluorescence images show cells in the ASP. Arrow points to EGFP droplet. T → A, the phosphothreonine of ERK-SPARK is changed to alanine; $FGFR^{DN}$, a dominant-negative mutant of FGFR; HS-FGF, FGF level was elevated through a brief induction by heat shock (HS).

(B) Left: schematic diagrams of the wing imaginal disc and the EGFR/ERK-signaling pathway. Right: fluorescence images show cells in the wing pouch of the wing imaginal disc. T → A, the phosphothreonine of ERK-SPARK is changed to alanine (the image is 5× brightened relative to the left panel).

(C) Top: schematic of an adult wing with veins labeled. Bottom: images show adult wings developed from wing discs expressing ERK-SPARK versus a control. Scale bars, 25 (A)and 50 μm (B).

compared dpERK staining in discs that expressed ERK-SPARK with control discs, and we did not detect an apparent difference (Figure S9A).

Lastly, to examine if the expression of ERK-SPARK affects animal development, we compared the adult wings that are developed from wing imaginal discs. Flies expressing ERK-SPARK developed normal wings that were indistinguishable from wings of control flies (Figure 5C). This suggests that ERK-SPARK does not perturb wing development and is consistent with the dpERK staining that showed no apparent difference between the control and the ERK-SPARK-expressing flies. We further examined viability of the transgenic fly, which was not affected when ERK-SPARK was expressed in the trachea or in the whole animal (Figure S9B). These results suggest that ERK-SPARK is a valid indicator of ERK activity in animal tissues.

To demonstrate PKA-SPARK, we expressed the reporter in the wing imaginal discs, and we observed that cells in the pouch region of the wing discs had evenly distributed green fluorescence (Figure S9C), suggesting expression of the reporter. We then expressed a constitutively active form of the alpha subunit

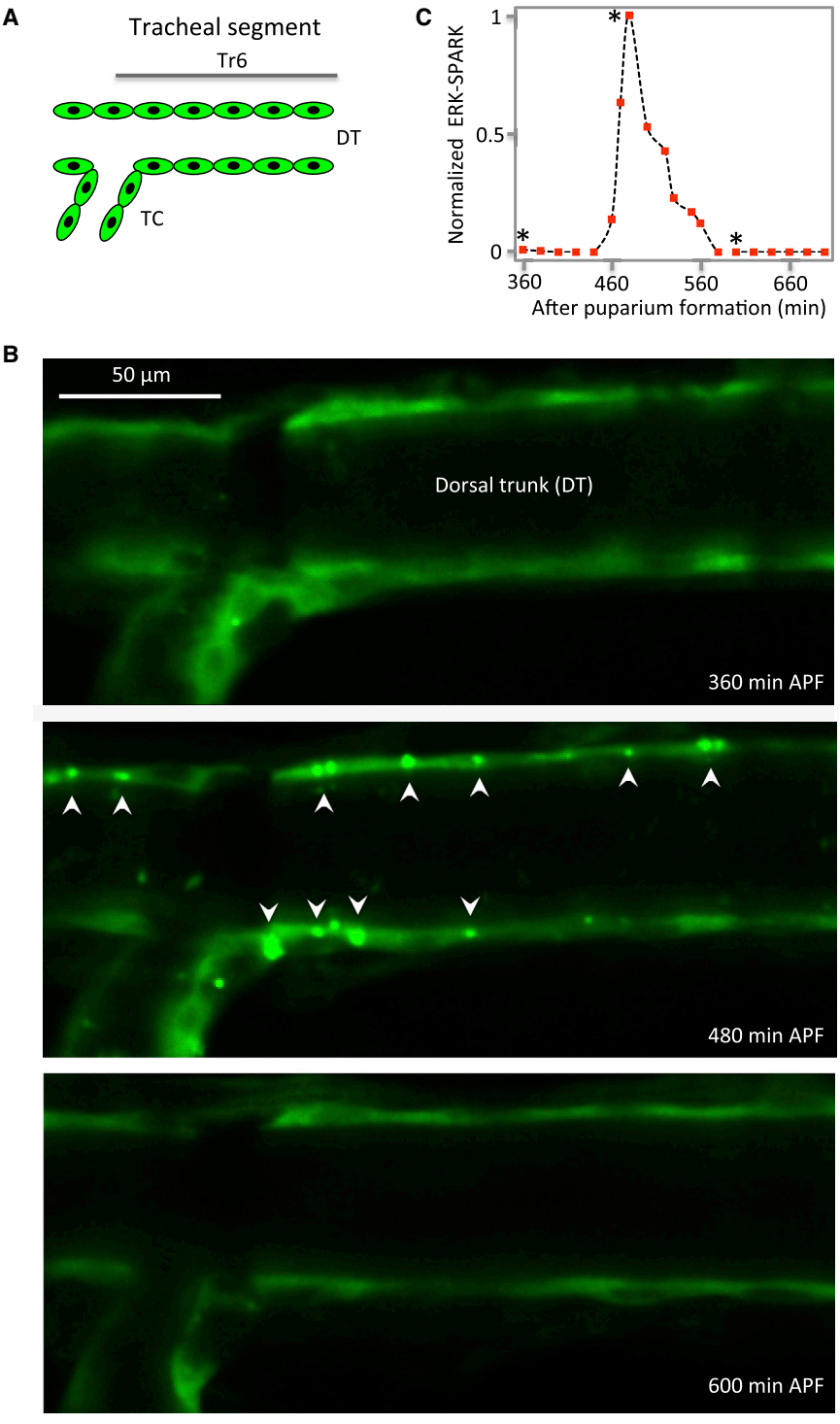


**Figure 6. ERK-SPARK Can Be Used in Live Imaging to Visualize Dynamics of ERK Signaling *In Vivo***

(A) Schematic diagram of the *Drosophila* trachea. Left: tracheal metamere (Tr) 6 is shown. DT, dorsal trunk; TC, transverse connective branch.

(B) Time-lapse fluorescence images of the trachea in intact *Drosophila* pupa. ERK-SPARK was expressed by crossing the UAS-ERK-SPARK transgenic fly with the btl-GAL4 line. Arrowhead points to EGFP droplets.

(C) Normalized ERK-SPARK signal over time. Stars correspond to images in (B).

Scale bar, 50 μm (B).

of stimulatory G protein (Gαs*), which activates AC for cAMP production and results in PKA activation (Quan et al., 1991; Wolfgang et al., 1996). EGFP droplets were detected in the wing discs subsequent to ectopic expression of Gαs* (Figure S9D). We conclude that PKA-SPARK enables visualization of PKA activity in the *Drosophila* tissue.

## SPARK Can Be Used in Live Imaging to Visualize the Dynamics of ERK Signaling *In Vivo*

Live imaging of kinase activities in animals such as *Drosophila* is technically challenging due to the small dynamic range of the previous reporters and optical issues, such as tissue autofluorescence and light scattering as well as rapid cell movements and shape changes (Kardash et al., 2011). Since the SPARK reporters have a large dynamic range and a simple signal pattern that is readily detected, they may enable imaging of dynamic kinase activity in developing animals. To determine whether ERK-SPARK could be used in live imaging to visualize dynamics of ERK signaling during animal development (Shilo, 2014; Sopko and Perrimon, 2013), we focused on the tracheal system, which is accessible to live imaging and given that FGFR/ERK signaling plays a critical role in tracheal development during metamorphosis at the pupal stage (Chen and Krasnow, 2014), but the dynamics of ERK signaling are unknown. To visualize ERK signaling, we expressed ERK-SPARK in the tracheal cells by crossing the UAS-ERK-SPARK line with the *btl*-GAL4 line.

Time-lapse fluorescence imaging of the trachea between 6 and 11 hr after puparium formation (APF) revealed transient ERK signaling (Figures 6A and 6B). First, EGFP green fluorescence was observed along the dorsal trunk, indicating that ERK-SPARK is expressed in the tracheal cells. Few EGFP droplets were detected between 6 and 7.5 hr APF. Abundant EGFP droplets appeared between 7.5 and 9.5 hr APF, indicating that ERK was activated in the tracheal cells during this period. In the following 2 hr, few EGFP droplets were detected, suggesting that ERK was inactivated. Our imaging results thus indicate that ERK activity was transiently activated in

the trachea between 6 and 11 hr APF (Figure 6C; Movie S11). Our work thus demonstrates that the SPARK kinase reporter can be used to visualize dynamic kinase signaling in a live animal during development. SPARK represents another class of fluorescent reporters for imaging kinase-signaling dynamics in animals. The SPARK reporters will find important biological applications in small animals, including *Drosophila* and zebrafish (Figure S10).

### The SPARK Technology Can Be Employed to Develop Reporters of Other Kinases

The SPARK technology is based on multivalent PPI-induced phase separation and formation of fluorescent droplets. While the multivalency is introduced by the paired HOTags, the PPI is based on two modular motifs: the kinase-specific substrate domain and the phosphopeptide-binding domain (PBD). The PPI motifs in the SPARK technology are compatible with most FRET-based kinase reporters since they also use these two motifs to sense kinase activity. Therefore, the kinase activity-sensing motifs from the FRET reporters can likely be utilized to develop phase separation-based reporters of many kinases (Oldach and Zhang, 2014). In general, the kinase activity-sensing motif can be adapted from specific kinase substrates to develop the SPARK technology-based kinase reporters, and the PBD may be obtained from the proteins that bind phosphorylated substrates.

In summary, we have developed phase separation-based kinase reporters, SPARKs, which achieve large fluorescence increase, high brightness, and fast kinetics. Because of intensive fluorescence, simple signal pattern, and rapid response, SPARKs enable easy and robust visualization of dynamic kinase signaling in living animals in a qualitative way, based on raw images with no requirement for quantitative data analysis. Because of the modular design, other fluorescent proteins may be used to develop multicolor SPARK for other contexts. Furthermore, development of other homo-oligomeric coiled coils that are orthogonal to HOTag3/6 will enable simultaneous imaging of multiple kinase activities. Such multicolor SPARKs could be valuable tools for visualizing signaling networks in living animals.

### Limitations

The main limitation of the SPARK technology is spatial resolution, which is poorer than the FRET-based kinase reporters. On the other hand, compared to the KTR-based kinase reporters, its spatial resolution is better since, in principle, it can distinguish kinase activities in the cytoplasm versus nucleus.

## STAR★METHODS

Detailed methods are provided in the online version of this paper and include the following:

- KEY RESOURCES TABLE
- CONTACT FOR REAGENT AND RESOURCE SHARING
- EXPERIMENTAL MODEL AND SUBJECT DETAILS
  - Animals
  - Cell culture
- METHOD DETAILS
  - Plasmid construction
  - Characterization of HOTags in mammalian cells
  - Live cell imaging
  - Live zebrafish imaging
  - Estimation of absolute concentrations of EGFP in cells
- QUANTIFICATION AND STATISTICAL ANALYSIS
  - Image analysis
  - *Drosophila* viability quantification

### SUPPLEMENTAL INFORMATION

Supplemental Information includes 10 figures and 11 movies and can be found with this article online at https://doi.org/10.1016/j.molcel.2017.12.008.

### ACKNOWLEDGMENTS

This work was supported by NIH Director's New Innovator Award 1DP2GM105446 (to X.S.), R01 HL054737 and R01 HL121387 (to S.R.C.), R35 GM122548 (to T.B.K.), and 5T32HL007731 (to H.H.). We thank Wendell Lim for constructive comments; Dr. Lani Wu for discussion of data analysis; and Drs. Ken-ichi Kimura, Benny Shilo, and Markus Affolter and the Bloomington *Drosophila* Stock Center and the Vienna *Drosophila* RNAi Center for sharing fly stocks.

### AUTHOR CONTRIBUTIONS

X.S. conceived the project. X.S. designed the reporters. Q.Z. made the constructs, conducted fluorescence imaging, and characterized the reporters. T.B.K. and H.H. designed the *Drosophila* experiments. S.R.C., R.W., and A.S. designed the zebrafish experiments. Q.Z., H.H., Q.L., R.W., C.I.C., J.T., S.-Q.Z., and A.S. performed the experiments. X.S., Q.Z., and H.H. wrote the manuscript. All authors contributed to the final draft.

### DECLARATION OF INTERESTS

The authors declare no competing interests.

Received: May 6, 2017
Revised: July 18, 2017
Accepted: December 7, 2017
Published: January 4, 2018

### REFERENCES

Banani, S.F., Rice, A.M., Peeples, W.B., Lin, Y., Jain, S., Parker, R., and Rosen, M.K. (2016). Compositional Control of Phase-Separated Cellular Bodies. Cell *166*, 651–663.

Banani, S.F., Lee, H.O., Hyman, A.A., and Rosen, M.K. (2017). Biomolecular condensates: organizers of cellular biochemistry. Nat. Rev. Mol. Cell Biol. *18*, 285–298.

Banaszynski, L.A., Liu, C.W., and Wandless, T.J. (2005). Characterization of the FKBP.rapamycin.FRB ternary complex. J. Am. Chem. Soc. *127*, 4715–4721.

Chen, F., and Krasnow, M.A. (2014). Progenitor outgrowth from the niche in Drosophila trachea is guided by FGF from decaying branches. Science *343*, 186–189.

Chen, J.-F., Eltzschig, H.K., and Fredholm, B.B. (2013). Adenosine receptors as drug targets–what are the challenges? Nat. Rev. Drug Discov. *12*, 265–286.

Coughlin, S.R. (2000). Thrombin signalling and protease-activated receptors. Nature *407*, 258–264.

DeFea, K.A., Zalevsky, J., Thoma, M.S., Déry, O., Mullins, R.D., and Bunnett, N.W. (2000). beta-arrestin-dependent endocytosis of proteinase-activated receptor 2 is required for intracellular targeting of activated ERK1/2. J. Cell Biol. *148*, 1267–1281.

Doupé, D.P., and Perrimon, N. (2014). Visualizing and manipulating temporal signaling dynamics with fluorescence-based tools. Sci. Signal. *7*, re1.

Durocher, D., Taylor, I.A., Sarbassova, D., Haire, L.F., Westcott, S.L., Jackson, S.P., Smerdon, S.J., and Yaffe, M.B. (2000). The molecular basis of FHA domain:phosphopeptide binding specificity and implications for phospho-dependent signaling mechanisms. Mol. Cell *6*, 1169–1182.

Fairclough, R.H., and Cantor, C.R. (1978). The use of singlet-singlet energy transfer to study macromolecular assemblies. Methods Enzymol. *48*, 347–379.

Fredholm, B.B., Bättig, K., Holmén, J., Nehlig, A., and Zvartau, E.E. (1999). Actions of caffeine in the brain with special reference to factors that contribute to its widespread use. Pharmacol. Rev. *51*, 83–133.

Gabay, L., Seger, R., and Shilo, B.Z. (1997). In situ activation pattern of Drosophila EGF receptor pathway during development. Science *277*, 1103–1106.

Grigoryan, G., Kim, Y.H., Acharya, R., Axelrod, K., Jain, R.M., Willis, L., Drndic, M., Kikkawa, J.M., and DeGrado, W.F. (2011). Computational design of virus-like protein assemblies on carbon nanotube surfaces. Science *332*, 1071–1076.

Harvey, C.D., Ehrhardt, A.G., Cellurale, C., Zhong, H., Yasuda, R., Davis, R.J., and Svoboda, K. (2008). A genetically encoded fluorescent sensor of ERK activity. Proc. Natl. Acad. Sci. USA *105*, 19264–19269.

Higley, M.J., and Sabatini, B.L. (2010). Competitive regulation of synaptic Ca2+ influx by D2 dopamine and A2A adenosine receptors. Nat. Neurosci. *13*, 958–966.

Huang, P.-S., Oberdorfer, G., Xu, C., Pei, X.Y., Nannenga, B.L., Rogers, J.M., DiMaio, F., Gonen, T., Luisi, B., and Baker, D. (2014). High thermodynamic stability of parametrically designed helical bundles. Science *346*, 481–485.

Hunter, T. (2009). Tyrosine phosphorylation: thirty years and counting. Curr. Opin. Cell Biol. *21*, 140–146.

Hyman, A.A., Weber, C.A., and Jülicher, F. (2014). Liquid-liquid phase separation in biology. Annu. Rev. Cell Dev. Biol. *30*, 39–58.

Hynes, N.E., Ingham, P.W., Lim, W.A., Marshall, C.J., Massagué, J., and Pawson, T. (2013). Signalling change: signal transduction through the decades. Nat. Rev. Mol. Cell Biol. *14*, 393–398.

Jazayeri, A., Andrews, S.P., and Marshall, F.H. (2017). Structurally Enabled Discovery of Adenosine A2A Receptor Antagonists. Chem. Rev. *117*, 21–37.

Kardash, E., Bandemer, J., and Raz, E. (2011). Imaging protein activity in live embryos using fluorescence resonance energy transfer biosensors. Nat. Protoc. *6*, 1835–1846.

Komatsu, N., Aoki, K., Yamada, M., Yukinaga, H., Fujita, Y., Kamioka, Y., and Matsuda, M. (2011). Development of an optimized backbone of FRET biosensors for kinases and GTPases. Mol. Biol. Cell *22*, 4647–4656.

Lebon, G., Warne, T., Edwards, P.C., Bennett, K., Langmead, C.J., Leslie, A.G., and Tate, C.G. (2011). Agonist-bound adenosine A2A receptor structures reveal common features of GPCR activation. Nature *474*, 521–525.

Lee, T., Hoofnagle, A.N., Kabuyama, Y., Stroud, J., Min, X., Goldsmith, E.J., Chen, L., Resing, K.A., and Ahn, N.G. (2004). Docking motif interactions in MAP kinases revealed by hydrogen exchange mass spectrometry. Mol. Cell *14*, 43–55.

Lefkowitz, R.J., and Shenoy, S.K. (2005). Transduction of receptor signals by beta-arrestins. Science *308*, 512–517.

Lemmon, M.A., and Schlessinger, J. (2010). Cell signaling by receptor tyrosine kinases. Cell *141*, 1117–1134.

Li, P., Banjade, S., Cheng, H.-C., Kim, S., Chen, B., Guo, L., Llaguno, M., Hollingsworth, J.V., King, D.S., Banani, S.F., et al. (2012). Phase transitions in the assembly of multivalent signalling proteins. Nature *483*, 336–340.

Luttrell, L.M., Roudabush, F.L., Choy, E.W., Miller, W.E., Field, M.E., Pierce, K.L., and Lefkowitz, R.J. (2001). Activation and targeting of extracellular signal-regulated kinases by beta-arrestin scaffolds. Proc. Natl. Acad. Sci. USA *98*, 2449–2454.

Manning, G., Whyte, D.B., Martinez, R., Hunter, T., and Sudarsanam, S. (2002). The protein kinase complement of the human genome. Science *298*, 1912–1934.

Marshall, C.J. (1995). Specificity of receptor tyrosine kinase signaling: transient versus sustained extracellular signal-regulated kinase activation. Cell *80*, 179–185.

Miyawaki, A., and Niino, Y. (2015). Molecular spies for bioimaging–fluorescent protein-based probes. Mol. Cell *58*, 632–643.

Mo, G.C.H., Ross, B., Hertel, F., Manna, P., Yang, X., Greenwald, E., Booth, C., Plummer, A.M., Tenner, B., Chen, Z., et al. (2017). Genetically encoded biosensors for visualizing live-cell biochemical activity at super-resolution. Nat. Methods *14*, 427–434.

Ohta, A., Gorelik, E., Prasad, S.J., Ronchese, F., Lukashev, D., Wong, M.K.K., Huang, X., Caldwell, S., Liu, K., Smith, P., et al. (2006). A2A adenosine receptor protects tumors from antitumor T cells. Proc. Natl. Acad. Sci. USA *103*, 13132–13137.

Oldach, L., and Zhang, J. (2014). Genetically encoded fluorescent biosensors for live-cell visualization of protein phosphorylation. Chem. Biol. *21*, 186–197.

Pawson, T., and Scott, J.D. (2005). Protein phosphorylation in signaling–50 years and counting. Trends Biochem. Sci. *30*, 286–290.

Purvis, J.E., and Lahav, G. (2013). Encoding and decoding cellular information through signaling dynamics. Cell *152*, 945–956.

Quan, F., Thomas, L., and Forte, M. (1991). Drosophila stimulatory G protein alpha subunit activates mammalian adenylyl cyclase but interacts poorly with mammalian receptors: implications for receptor-G protein interaction. Proc. Natl. Acad. Sci. USA *88*, 1898–1902.

Regot, S., Hughey, J.J., Bajar, B.T., Carrasco, S., and Covert, M.W. (2014). High-sensitivity measurements of multiple kinase activities in live single cells. Cell *157*, 1724–1734.

Reichman-Fried, M., and Shilo, B.Z. (1995). Breathless, a Drosophila FGF receptor homolog, is required for the onset of tracheal cell migration and tracheole formation. Mech. Dev. *52*, 265–273.

Rodriguez, E.A., Campbell, R.E., Lin, J.Y., Lin, M.Z., Miyawaki, A., Palmer, A.E., Shu, X., Zhang, J., and Tsien, R.Y. (2017). The Growing and Glowing Toolbox of Fluorescent and Photoactive Proteins. Trends Biochem. Sci. *42*, 111–129.

Sanford, L., and Palmer, A. (2017). Recent Advances in Development of Genetically Encoded Fluorescent Sensors (Elsevier Inc.).

Santos, S.D.M., Verveer, P.J., and Bastiaens, P.I.H. (2007). Growth factor-induced MAPK network topology shapes Erk response determining PC-12 cell fate. Nat. Cell Biol. *9*, 324–330.

Sasagawa, S., Ozaki, Y., Fujita, K., and Kuroda, S. (2005). Prediction and validation of the distinct dynamics of transient and sustained ERK activation. Nat. Cell Biol. *7*, 365–373.

Sato, M., and Kornberg, T.B. (2002). FGF is an essential mitogen and chemoattractant for the air sacs of the Drosophila tracheal system. Dev. Cell *3*, 195–207.

Shaner, N.C., Campbell, R.E., Steinbach, P.A., Giepmans, B.N.G., Palmer, A.E., and Tsien, R.Y. (2004). Improved monomeric red, orange and yellow fluorescent proteins derived from Discosoma sp. red fluorescent protein. Nat. Biotechnol. *22*, 1567–1572.

Sheridan, D.L., Kong, Y., Parker, S.A., Dalby, K.N., and Turk, B.E. (2008). Substrate discrimination among mitogen-activated protein kinases through distinct docking sequence motifs. J. Biol. Chem. *283*, 19511–19520.

Shilo, B.-Z. (2014). The regulation and functions of MAPK pathways in Drosophila. Methods *68*, 151–159.

Shin, Y., Berry, J., Pannucci, N., Haataja, M.P., Toettcher, J.E., and Brangwynne, C.P. (2017). Spatiotemporal Control of Intracellular Phase Transitions Using Light-Activated optoDroplets. Cell *168*, 159–171.e14.

Sopko, R., and Perrimon, N. (2013). Receptor tyrosine kinases in Drosophila development. Cold Spring Harb. Perspect. Biol. *5*, a009050.

Sturtevant, M.A., O'Neill, J.W., and Bier, E. (1994). Down-regulation of Drosophila Egf-r mRNA levels following hyperactivated receptor signaling. Development *120*, 2593–2600.

Taylor, S.S., Ilouz, R., Zhang, P., and Kornev, A.P. (2012). Assembly of allosteric macromolecular switches: lessons from PKA. Nat. Rev. Mol. Cell Biol. *13*, 646–658.

Thomson, A.R., Wood, C.W., Burton, A.J., Bartlett, G.J., Sessions, R.B., Brady, R.L., and Woolfson, D.N. (2014). Computational design of water-soluble $\alpha$-helical barrels. Science *346*, 485–488.

Toettcher, J.E., Weiner, O.D., and Lim, W.A. (2013). Using optogenetics to interrogate the dynamic control of signal transmission by the Ras/Erk module. Cell *155*, 1422–1434.

Tsien, R.Y. (1998). The green fluorescent protein. Annu. Rev. Biochem. *67*, 509–544.

Tsien, R.Y. (2009). Constructing and exploiting the fluorescent protein paintbox (Nobel Lecture). Angew. Chem. Int. Ed. Engl. *48*, 5612–5626.

Vu, T.K., Hung, D.T., Wheaton, V.I., and Coughlin, S.R. (1991a). Molecular cloning of a functional thrombin receptor reveals a novel proteolytic mechanism of receptor activation. Cell *64*, 1057–1068.

Vu, T.K., Wheaton, V.I., Hung, D.T., Charo, I., and Coughlin, S.R. (1991b). Domains specifying thrombin-receptor interaction. Nature *353*, 674–677.

Waters, J.C. (2009). Accuracy and precision in quantitative fluorescence microscopy. J. Cell Biol. *185*, 1135–1148.

Wolfgang, W.J., Roberts, I.J., Quan, F., O'Kane, C., and Forte, M. (1996). Activation of protein kinase A-independent pathways by Gs alpha in Drosophila. Proc. Natl. Acad. Sci. USA *93*, 14542–14547.

Woolfson, D.N., Bartlett, G.J., Burton, A.J., Heal, J.W., Niitsu, A., Thomson, A.R., and Wood, C.W. (2015). De novo protein design: how do we expand into the universe of possible protein structures? Curr. Opin. Struct. Biol. *33*, 16–26.

Yu, D., Baird, M.A., Allen, J.R., Howe, E.S., Klassen, M.P., Reade, A., Makhijani, K., Song, Y., Liu, S., Murthy, Z., et al. (2015). A naturally monomeric infrared fluorescent protein for protein labeling in vivo. Nat. Methods *12*, 763–765.

Zhang, J., Ma, Y., Taylor, S.S., and Tsien, R.Y. (2001). Genetically encoded reporters of protein kinase A activity reveal impact of substrate tethering. Proc. Natl. Acad. Sci. USA *98*, 14997–15002.

Zhang, J., Hupfeld, C.J., Taylor, S.S., Olefsky, J.M., and Tsien, R.Y. (2005). Insulin disrupts beta-adrenergic signalling to protein kinase A in adipocytes. Nature *437*, 569–573.

# STAR★METHODS

## KEY RESOURCES TABLE

| REAGENT or RESOURCE | SOURCE | IDENTIFIER |
|---|---|---|
| Chemicals, Peptides, and Recombinant Proteins | | |
| Calcium Phosphate Transfection Kit | ThermoFisher Scientific | CAT# K278001 |
| Lipofectamine 2000 Transfection Reagent | ThermoFisher Scientific | SKU#11668-019 |
| Isoproterenol | Sigma-Aldrich | 1351005; CAS: 51-30-9 |
| Ser-Phe-Leu-Leu-Arg-Asn-amide trifluoroacetate salt [PAR-1 (Protease-Activated Receptor) Selective Activating Peptide] | Sigma-Aldrich | S1820; CAS: 141923-40-2 (free base) |
| Carvedilol | Sigma-Aldrich | C3993; CAS: 72956-09-3 |
| Adenosine | Sigma-Aldrich | A9251; CAS: 58-61-7 |
| Caffeine | Sigma-Aldrich | C0750; CAS:58-08-2 |
| JNK Inhibitor VIII | Sigma-Aldrich | 420135; CAS 894804-07-0 |
| P38 inhibitor, SB 203580 | Sigma-Aldrich | S8307; CAS: 152121-47-6 |
| ERK inhibitor, PD 0325901 | Sigma-Aldrich | PZ0162 ; CAS: 391210-10-9 |
| H-89 dihydrochloride hydrate | Sigma-Aldrich | B1427; CAS:130964-39-5 (anhydrous) |
| Experimental Models: Cell Lines | | |
| 293T/17 | ATCC | CRL-11268 |
| Experimental Models: Organisms/Strains | | |
| *D. melanogaster*: Wild type: w1118 | Bloomington *Drosophila* Stock Center | BDSC: 3605 |
| *D. melanogaster*: *btl-GAL4* | Sato and Kornberg, 2002 | N/A |
| *D. melanogaster*: *hs-FGF* | Sato and Kornberg, 2002 | N/A |
| *D. melanogaster*: *UAS-FGFR$^{DN}$* | Reichman-Fried and Shilo, 1995 | N/A |
| *D. melanogaster*: *tub-Gal4* | Bloomington *Drosophila* Stock Center | BDSC:5138 |
| *D. melanogaster*: PKA-SPARK | This paper | N/A |
| *D. melanogaster*: ERK-SPARK | This paper | N/A |
| *D. melanogaster*: ERK-SPARK (T mutated to A) | This paper | N/A |
| Recombinant DNA | | |
| Plasmid: H2B-mIFP | Yu et al., 2015 | Addgene: 56223 |
| Plasmid: mCherry | Shaner et al., 2004 | |
| Plasmid: pcDNA3-FKBP-EGFP-HOTag1 | This paper | N/A |
| Plasmid: pcDNA3-FKBP-EGFP-HOTag2 | This paper | N/A |
| Plasmid: pcDNA3-FKBP-EGFP-HOTag3 | This paper | N/A |
| Plasmid: pcDNA3-FKBP-EGFP-HOTag4 | This paper | N/A |
| Plasmid: pcDNA3-FKBP-EGFP-HOTag5 | This paper | N/A |
| Plasmid: pcDNA3-FKBP-EGFP-HOTag6 | This paper | N/A |
| Plasmid: pcDNA3-FKBP-EGFP-HOTag7 | This paper | N/A |
| Plasmid: pcDNA3-Frb-EGFP-HOTag1 | This paper | N/A |
| Plasmid: pcDNA3-Frb-EGFP-HOTag2 | This paper | N/A |
| Plasmid: pcDNA3-Frb-EGFP-HOTag3 | This paper | N/A |
| Plasmid: pcDNA3-Frb-EGFP-HOTag4 | This paper | N/A |
| Plasmid: pcDNA3-Frb-EGFP-HOTag5 | This paper | N/A |
| Plasmid: pcDNA3-Frb-EGFP-HOTag6 | This paper | N/A |
| Plasmid: pcDNA3-Frb-EGFP-HOTag7 | This paper | N/A |
| Plasmid: pcDNA3-LRRATLVD-EGFP-HOTag3 2A FHA1-HOTag6 (i.e., PKA-SPARK) | This paper | N/A |

(*Continued on next page*)

*Continued*

| REAGENT or RESOURCE | SOURCE | IDENTIFIER |
|---|---|---|
| Plasmid: pcDNA3-LRRAALVD-EGFP-HOTag3 2A FHA1-HOTag6 | This paper | N/A |
| Plasmid: pcDNA3-PDVPRTPVDKAKLSFQFP-EGFP-HOTag3 2A WW-EGFP-HOTag6 (i.e., ERK-SPARK) | This paper | N/A |
| Plasmid: pcDNA3-PDVPRAPVDKAKLSFQFP-EGFP-HOTag3 2A WW-EGFP-HOTag6 | This paper | N/A |
| Plasmid: pcDNA3-PDVPRTPVDKAKLS-EGFP-HOTag3 2A WW-EGFP-HOTag6 | This paper | N/A |
| Plasmid: pIHEU-LRRATLVD-EGFP-HOTag3 2A FHA1-HOTag6 (PKA-SPARK for expression in *Drosophila*) | This paper | N/A |
| Plasmid: pIHEU-PDVPRTPVDKAKLSFQFP-EGFP-HOTag3 2A WW-EGFP-HOTag6 (ERK-SPARK for expression in *Drosophila*) | This paper | N/A |
| Plasmid: pIHEU-PDVPRAPVDKAKLSFQFP-EGFP-HOTag3 2A WW-EGFP-HOTag6 | This paper | N/A |
| Plasmid: pminiTol2-LRRATLVD-EGFP-HOTag3 2A FHA1-HOTag6 (PKA-SPARK for expression in zebrafish) | This paper | N/A |
| Software and Algorithms | | |
| NIS-Element | Nikon | N/A |
| Fiji ImageJ | Open | https://fiji.sc/ |

## CONTACT FOR REAGENT AND RESOURCE SHARING

Further information and requests for reagents may be directed to, and will be fulfilled by, the Lead Contact, Xiaokun Shu (Xiaokun.shu@ucsf.edu).

## EXPERIMENTAL MODEL AND SUBJECT DETAILS

### Animals

*D. melanogaster w1118* was used as the wild-type strain. Fly crosses were maintained at 25°C. The *Drosophila* transgenic lines were generated in this study by using attP insertion on 3$^{rd}$ chromosome.

### Cell culture

The HEK293T/17 cells were passaged in Dulbecco's Modified Eagle medium (DMEM) supplemented with 10% Fetal Bovine Serum (FBS), non-essential amino acids, penicillin (100 units/mL) and streptomycin (100 μg/mL). All culture supplies were obtained from the UCSF Cell Culture Facility.

## METHOD DETAILS

### Plasmid construction

All plasmid constructs were created by standard molecular biology techniques and confirmed by exhaustively sequencing the cloned fragments. To create FKBP-EGFP-HOTag fusions, FKBP was first cloned into pcDNA3 containing EGFP. Various HOTag (HOTag1 to HOTag7) was then each cloned into the pcDNA3 FKBP-EGFP construct, resulting in pcDNA3 FKBP-EGFP-HOTagX (X = 1, 2, 3, …, 7). Similar procedures were carried out to produce pcDNA3 Frb-EGFP-HOTagY (Y = 1, 2, 3, …, 7). To create PKA-SPARK, DNA fragments encoding LRRATLVD was inserted to replace FKBP in the pcDNA3 FKBP-EGFP-HOTag3 construct. DNA sequence encoding the FHA1 domain from the FRET-based PKA reporter AKAR was fused to HOTag6. A 2A sequence was added before the FHA1. The DNA fragment encoding 2A-FHA1-HOTag6 was then cloned into the pcDNA3 LRRATLVD-EGFP-HOTag3 to produce pcDNA3 LRRATLVD-EGFP-HOTag3 2A FHA1-HOTag6 (i.e., PKA-SPARK). To create ERK-SPARK, a DNA sequence encoding PDVPRTPVDKAKLSFQFP was introduced to replace FKBP in the pcDNA3 FKBP-EGFP-HOTag3 construct. The DNA sequence encoding WW domain was introduced to replace Frb in the pcDNA3 Frb-EGFP-HOTag6. The 2A sequence was then added before WW domain. The DNA fragment encoding 2A-WW-EGFP-HOTag6 was then cloned into the pcDNA3 PDVPRTPVDKAKLSFQFP-EGFP-HOTag3 to produce the final construct pcDNA3 PDVPRTPVDKAKLSFQFP-EGFP-HOTag3 2A WW-EGFP-HOTag6 (i.e., ERK-SPARK). The phosphothreonine was changed to alanine in the PKA-SPARK and ERK-SPARK using site-directed mutagenesis

(Agilent). To create plasmids for making transgenic *Drosophila*, the DNA fragement encoding PKA-SPARK or ERK-SPARK was cloned into pIHEU construct. To create plasmid for expression in zebrafish, PKA-SPARK was cloned into pminiTol2 construct.

### Characterization of HOTags in mammalian cells

To robustly induce protein phase separation or droplet formation via protein interaction, the HOTags should meet several requirements. First, HOTags themselves should not form protein droplets even at high concentration in cells. We therefore chose coiled coils that have been reported to be highly soluble. For example, the pentameric HOTag1 was previously shown to be soluble in aqueous solution (Huang et al., 2014). However, most of these *de novo* designed coiled coils were characterized using synthesized peptides and had not been expressed in mammalian cells. It was thus unclear whether they fold properly in the cellular context and whether they are soluble in mammalian cells. We transfected the fusion constructs (FKBP-EGFP-HOTag) into human embryonic kidney 293 (HEK293) cells, and fluorescence imaging indicated that HOTag3 and HOTag6 (Figure 1B), along with HOTag2, 5, and 7 (Figure S1B), were soluble even at high expression level (~20 μM [see "Estimation of absolute concentrations of EGFP in cells," Figure S2]). HOTag4 is not soluble at this high expression level, but it was soluble at ~10 μM (Figure S1B). HOTag1 was not soluble even at low expression level (~0.3 μM, Figure S1B). Thus, we decided to abandon HOTag1 and focus on the other six HOTags.

In order to achieve PPI-inducible protein phase separation, the second task was to identify pairs of HOTags that do not cross-interact to form protein droplets in the absence of PPI-induction. To find soluble HOTag pairs, we co-expressed two fusion constructs (FKBP-EGFP-HOTagX and Frb-EGFP-HOTagY) in HEK293 cells (Figure 1C; Figures S1C and S1D). Fluorescence imaging indicated that none of the fifteen pairs formed protein droplet at ~10 μM expression level in cells (Figure S1C). We then examined whether the fusion proteins could be induced to form droplets. Upon addition of rapamycin, time-lapse fluorescence imaging revealed that the pairs formed protein droplets at ~10 μM (Figures S1C and S1D). However, only two pairs, HOTag2/7 and HOTag3/6, formed droplets at ~1 μM (Figures S1C and S1D). At ~0.3 μM expression level, only the HOTag3/6 pair formed droplets upon rapamycin-induced PPI (Figures S1C and S1D). Therefore, our data indicate that the hexameric HOTag3 and the tetrameric HOTag6 (Figure S1E) can robustly drive protein phase separation upon protein interaction. We thus chose HOTag3/6 as the pair for use in kinase reporters.

### *Western blot of dually phosphorylated ERK*

Cells were lysed in 1X SDS sample buffer and resolved in NuPAGE 4%–12% Bis-Tris Protein Gels. After transferring, Phospho-p44/42 MAPK (Erk1/2) (Thr202/Tyr204) (D13.14.4E) Rabbit mAb (CST, 4370S) were used at 1:1000. HRP-Donkey-anti-Rabbit (Invitrogen A16029) antibodies were used at 1:10,000. Pierce ECL standard substrate buffer was used for visualization against film. The membrane was then stripped with Pierce Western Blot Stripping Buffer. HRP-anti-actin (Santa Cruz Biotechnology, sc-47778 HRP) was used at 1:10,000 for detecting beta-actin as a loading control.

### Drosophila *husbandry*

Flies were reared on standard cornmeal and agar medium at 25°C. The L3 wandering larvae were staged in cold PBS. Wing discs and associated trachea were immersed in a drop of PBS underneath a coverslip. A previously established fly line Btl-RFP-moe is used to specifically label the tracheal progenitors (Chen and Krasnow 2014). Btl-RFP-moe does not encompass the entire enhancer of breathless gene as btl-Gal4, but it turns out to be the best reagent to specifically label tracheal progenitor cells (Chen and Krasnow 2014).

### *Live* Drosophila *imaging*

White pupae of *Drosophila* (0hr APF) were brief washed and cleaned. Pupae were mounted within a drop of halocarbon oil 700 (Sigma) between two stripes of vacuum grease. Next, pupae were mixed well with oil, positioned with forceps and rolled so that a single trachea is up for optimal imaging of Tr4 and Tr5 metamere. Then, pupae were immobilized by a 22X30mm No.1.5 cover glass.

Fluorescence imaging was conducted on a Nikon Eclipse Ti inverted microscope equipped with a Yokogawa CSU-W1 confocal scanner unit (Andor), a digital CMOS camera ORCA-Flash4.0 (Hamamatsu), a ASI MS-2000 XYZ automated stage (Applied Scientific Instrumentation), a Nikon CFI Plan Apochromatic 20X dry (N.A. 0.75) objective, CFI apochromatic confocal LWD 40X WI λS water objective (N.A. 1.15), CFI apochromatic TIRF 60X oil objective (N.A. 1.49). Laser inputs were provided by an Integrated Laser Engine (Spectral Applied Research) equipped with laser lines (Coherent) 488 nm for GFP imaging, 561 nm for mCherry imaging, and 642 nm for mIFP imaging. The confocal scanning unit was equipped with the following emission filters: 525/50-nm for GFP imaging, 610/60-nm for mCherry imaging, 732/68-nm for mIFP imaging.

Fluorescence imaging of *Drosophila* larvae or pupae was carried out in an incubation chamber maintained at 25°C. The animals were imaged using a 20X dry objective for ~10 hours with image acquisition every 10 minutes.

### Live cell imaging

HEK293T/17 cells were transiently transfected with the plasmid using calcium phosphate transfection reagent or lipofectamine. Cells were grown in 35 mm glass bottom microwell (14 mm) dishes (MatTek Corporation). Transfection was performed when cells were cultured to ~50% confluence. For each transfection, 4.3 μg of plasmid DNA was mixed with 71 μL of 1X Hanks' Balanced Salts buffer (HBS) and 4.3 μL of 2.5M $CaCl_2$. Cells were imaged 24 hours after transient transfection.

Time-lapse imaging was performed with the aid of an environmental control unit incubation chamber (InVivo Scientific), which was maintained at 37°C and 5% $CO_2$. Fluorescence images were acquired with an exposure time of 50 ms for EGFP, 100 ms for mCherry, 200 ms for mIFP. Chemical reagents were carefully added to the cells in the incubation chamber when the time-lapse imaging was started. In particular, to induce interaction between FKBP and Frb, 100 nM rapamycin was added. To activate βARs, 10 μM

isoprenaline was added. To demonstrate specificity of PKA-SPARK, cells were pre-incubated with 10 μM H89 before addition of 10 μM isoprenaline. For inhibition of bARs, cells were incubated with 10 μM carvedilol for 5 minutes before addition of 2 μM isoprenaline. To demonstrate specificity of ERK-SPARK, cells were pre-incubated with 10 μM ERK inhibitor PD 0325901, or 10 μM JNK inhibitor VIII, or 10 μM p38 inhibitor SB 203580, before addition of 1 μM EGF. To activate PAR1, cells were stimulated with 10 μM PAR1 agonist SFLLRN. Image acquisition was controlled by the NIS-Elements Ar Microscope Imaging Software (Nikon). Images were processed using NIS-Elements and ImageJ (NIH).

For FRET imaging, cells were transfected with AKAR2 or EKAR. Isoprenaline was added to HEK293 cells expressing AKAR2. EGF was added to HEK293 cells transfected with EKAR. Images at CFP and YFP channel were taken using 405nm laser. The fluorescence images were processed in ImageJ.

### Live zebrafish imaging

To demonstrate whether PKA-SPARK can be used in zebrafish, we injected DNA encoding the reporter into zebrafish embryo at one-cell stage. Muscle cells at 24 hr APF were imaged upon addition of isoprenaline, which showed EGFP droplet formation. Our data thus suggests that PKA-SPARK visualizes activation of PKA in zebrafish. Therefore, the SPARK reporters can be used in imaging kinase activity in zebrafish.

### Estimation of absolute concentrations of EGFP in cells

To estimate concentration of expressed EGFP in HEK293 cells, we followed a method described in a previous study (Shin et al., 2017). We first purified EGFP and determined its concentration based on its absorbance and extinction coefficent. Then we prepared EGFP at various concentrations between 0.3 μM and 28 μM. Next we imaged the EGFP samples under the fluorescence microscope and recorded fluorescence intensity (counts/pixel) for each sample. The net intensity was determined after subtracting the dark background (without sample). The relationship between EGFP concentration and the net fluorescence intensity (counts/pixel) was plotted (Figure S2). To estimate EGFP concentration in HEK293 cells, we imaged the cells using the same imaging parameters including the laser power, exposure time, and magnification as those used for purified EGFP samples. The pixel intensity in each cell was averaged, which was subtracted by the intensity of a nearby dark area. The plotted curve was used to estimate EGFP concentration in HEK293 cells based on the net intensity.

## QUANTIFICATION AND STATISTICAL ANALYSIS

### Image analysis

For quantitative analysis of the SPARK signal, images were processed in imageJ. The sum of droplets pixel fluorescence intensity and the cells pixel intensity were scored using Analyze Particle function in imageJ.

### *Drosophila* viability quantification

In viability assay, the numbers of ERK-SPARK-expressing adults and their siblings with balancers were counted. The survival percentage was calculated as observed progeny carrying the ERK-SPARK to the expected number, that is, observed number of non-balancer progeny to the offspring with a balancer. The adult progeny were obtained from at least three independent crosses. The survival ratios were plotted as bar graph in Prism.

**Molecular Cell, Volume *69***

## Supplemental Information

# Visualizing Dynamics of Cell Signaling *In Vivo* with a Phase Separation-Based Kinase Reporter

**Qiang Zhang, Hai Huang, Qing Lu, Roland Wu, Chan-I Chung, Shao-Qing Zhang, Joaquim Torra, Antonino Schepis, Shaun R. Coughlin, Thomas B. Kornberg, and Xiaokun Shu**

## Supplemental Information

## Supplemental Figures

A

| | | | |
|---|---|---|---|
| HOTag1 (pentamer) | TQEDLLKKIMKLLKKQIKLLKKQIKMLKRLEKQ | HOTag5 (tetramer) | AEAESALEYAQQALEKAQLALQAARQALKA |
| HOTag2 (heptamer) | GEIAQALKEIAKALKEIAWALKEIAQALKG | HOTag6 (tetramer) | TLREIEELLRKIIEDSVRSVAELEDIEKWLKKI |
| HOTag3 (hexamer) | GEIAKSLKEIAKSLKEIAWSLKEIAKSLKG | HOTag7 (tetramer) | GELAAIKQELAAIKKELAAIKWELAAIKQGAG |
| HOTag4 (pentamer) | GKIEQILQKIEKILQKIEWILQKIEQILQG | | |

B

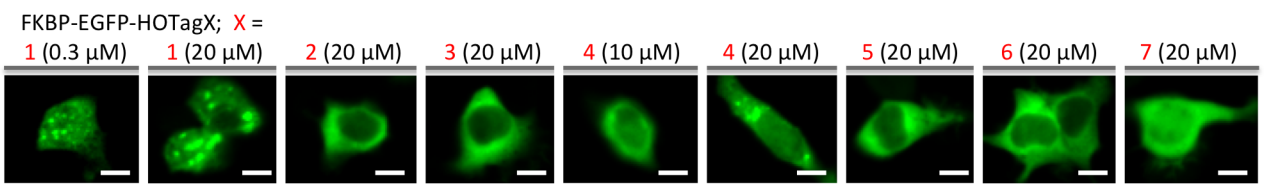


C

FKBP-EGFP-HOTagX + Frb-EGFP-HOTagY

| X = | 2 | | | | | 3 | | | | 4 | | | 5 | | 6 |
|---|---|---|---|---|---|---|---|---|---|---|---|---|---|---|---|
| Y = | 3 | 4 | 5 | 6 | 7 | 4 | 5 | 6 | 7 | 5 | 6 | 7 | 6 | 7 | 7 |
| Droplet? Rapamycin (−) | – | – | – | – | – | – | – | – | – | – | – | – | – | – | – |
| Droplet? Rapamycin (+) | + | + | + | + | ++ | + | + | +++ | + | + | + | + | + | + | + |

D

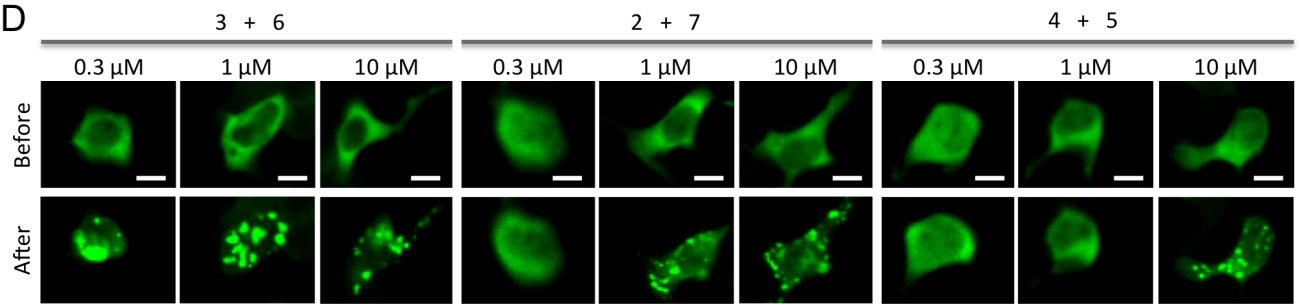


E

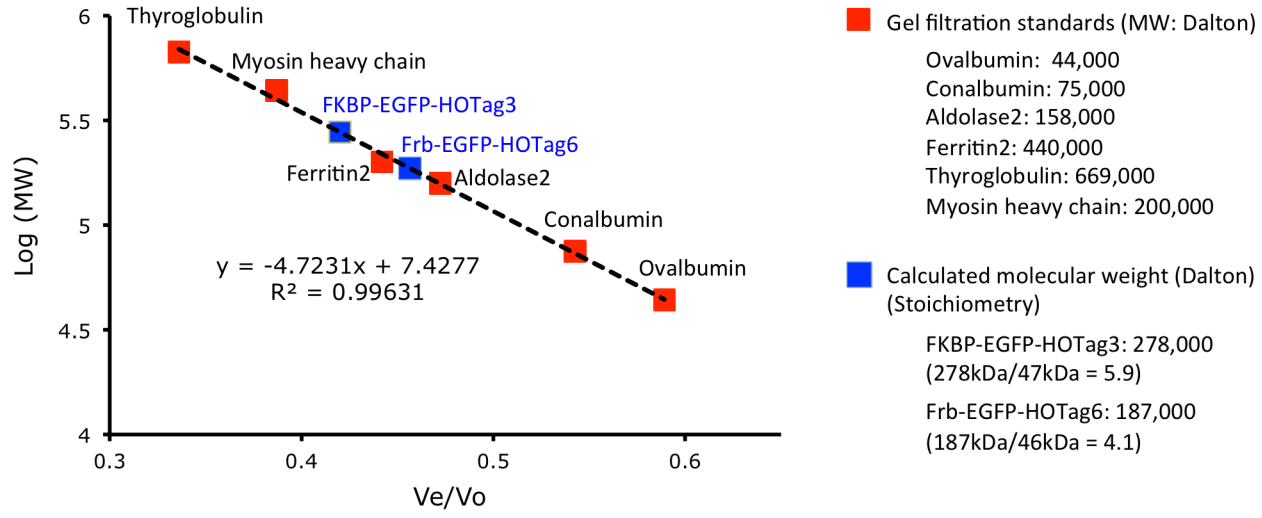

**Figure S1. Rational design of inducible protein phase separation by protein-protein interaction, Related to Figure 1**.

(A). *De novo* designed coiled coils are used as homo-oligomeric tag (HOTag), which introduces multivalency. (B). HOTags fused to EGFP and FKBP were expressed in HEK293 cells. (C). Protein concentration dependence of inducible droplet formation in HEK293 cells expressing combined HOTag fusions before and after rapamycin addition. −, no droplet. + denotes required protein expression level for droplet formation. +, 10 μM. ++, 1μM. +++, 0.3 μM. (D). Representative images showing EGFP droplet formation in HEK293 cells co-expressing pairs of HOTag fusions upon addition of rapamycin. Images were taken before and after rapamycin addition. (E). Determination of FKBP-EGFP-HOTag3 and Frb-EGFP-HOTag6 stoichiometry using size exclusion chromatography. A standard curve is drawn according to peak elution volume (Ve, elution volume; Vo, column volume) of the gel filtration standards as detected by absorption at 280 nm (red). The unit of MW in Y-axis is Dalton. The measured peak elution of the two fusion proteins are shown in blue. Molecular weight is calculated from the standard curve, which confirms that FKBP-EGFP-HOTag3 and Frb-EGFP-HOTag6 are hexameric and tetrameric, respectively. Scale bar, 10 μm.

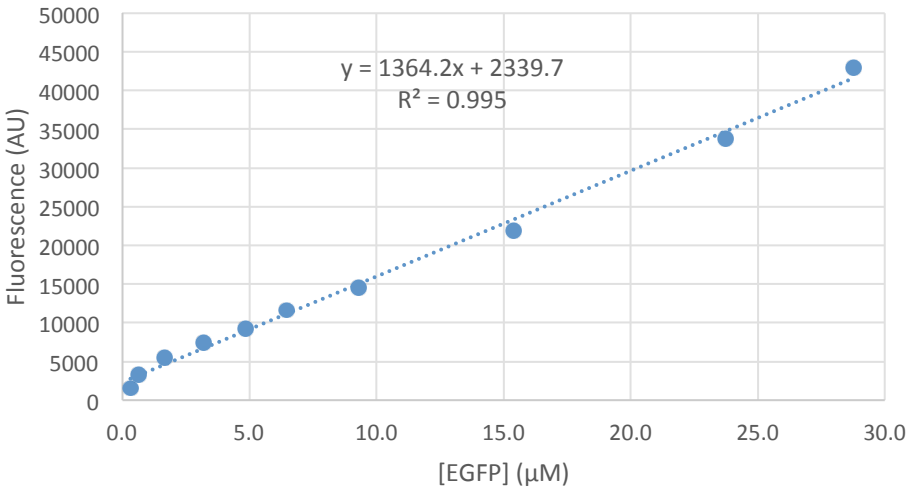


**Figure S2. Relationship of EGFP fluorescence brightness and concentration, Related to Star method**. EGFP was purified and aliquoted at various concentrations. The protein samples were then imaged under the confocal microscope. The fluorescence brightness was recorded, corresponding to EGFP concentration. The plotted line was used to estimate EGFP concentration in living cells based on the fluorescence brightness.

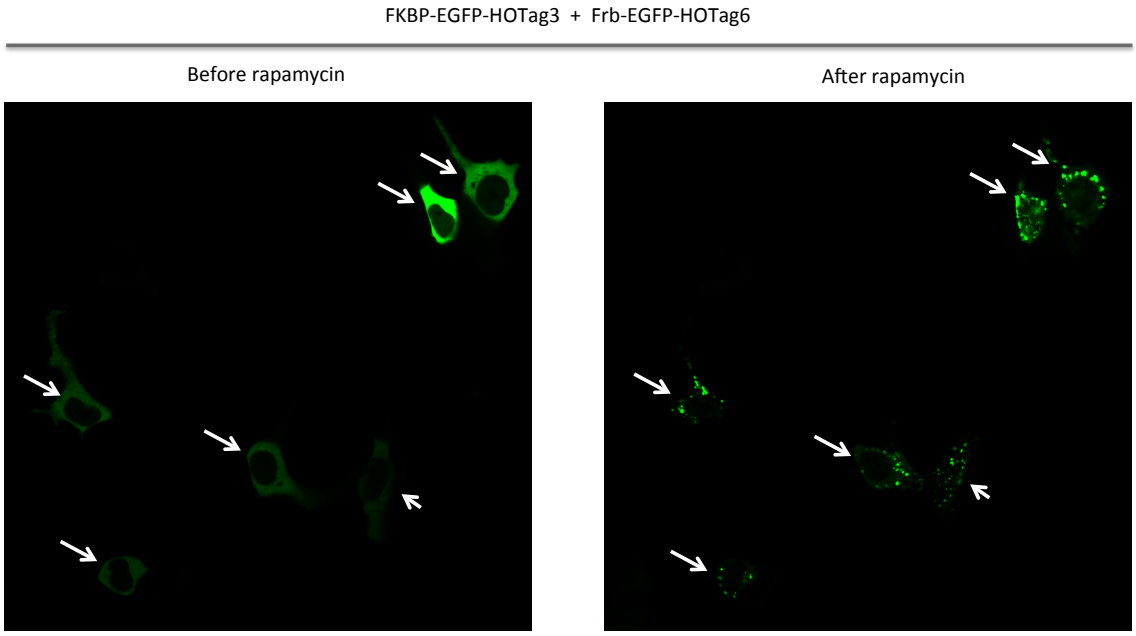


**Figure S3. Fluorescence images of HEK293 cells expressing FKBP-EGFP-HOTag3 and Frb-EGFP-HOTag6 upon addition of rapamycin, Related to Star method**.

Arrows point to individual cells.

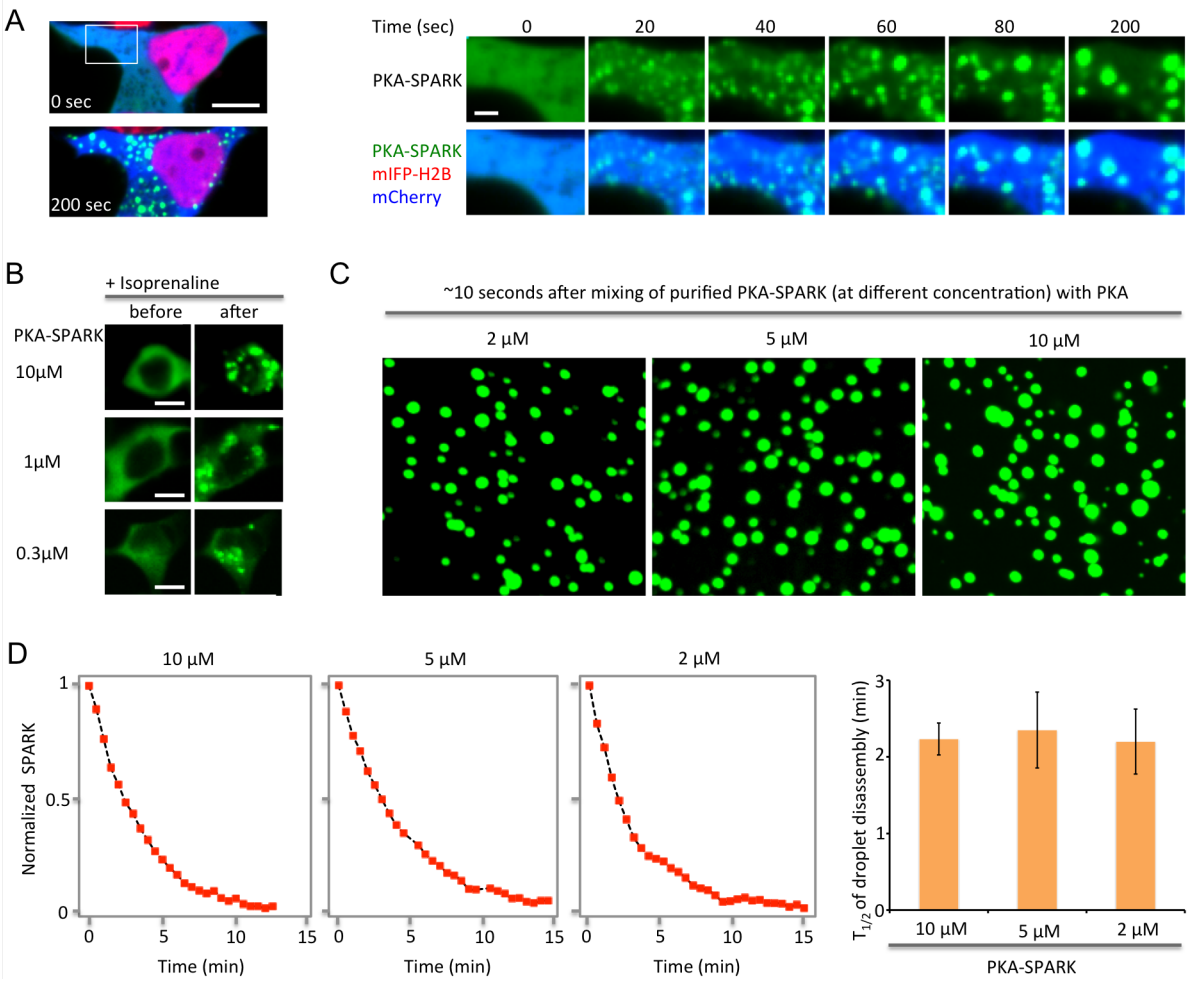


**Figure S4. Characterization of PKA-SPARK in HEK293 cells, Related to Figure 2**. (A). Time-lapse images of cells stimulated with isoprenaline. Cells expressing PKA-SPARK were also labeled with mCherry and a nucleus located monomeric infrared fluorescent protein (mIFP) fused to histone 2B (H2B). (B). Fluorescence images of cells expressing PKA-SPARK at various concentration. (C). Fluorescence images of purified PKA-SPARK mixed with PKA. Concentration dependence of PKA-SPARK droplet formation upon kinase activation was investigated. Images were taken immediately (~10 seconds) after mixing the purified PKA-SPARK (at specified concentration) with PKA (New England Biolabs). (D). Kinetics of PKA-SPARK droplet disassembly upon de-phosphorylation. Purified PKA-SPARK at specified concentration was pre-incubated with PKA to form droplets. Lambda protein phosphatase (New England Biolabs) was then added to the pre-formed PKA-SPARK droplets. The SPARK signal was calculated as described in the main text. The half time of droplet disassembly was plotted against the concentration of PKA-SPARK (right panel). Standard deviation was obtained from 3 independent measurements. Scale bar, A - B: 10 μm; right panel in A: 2 μm.

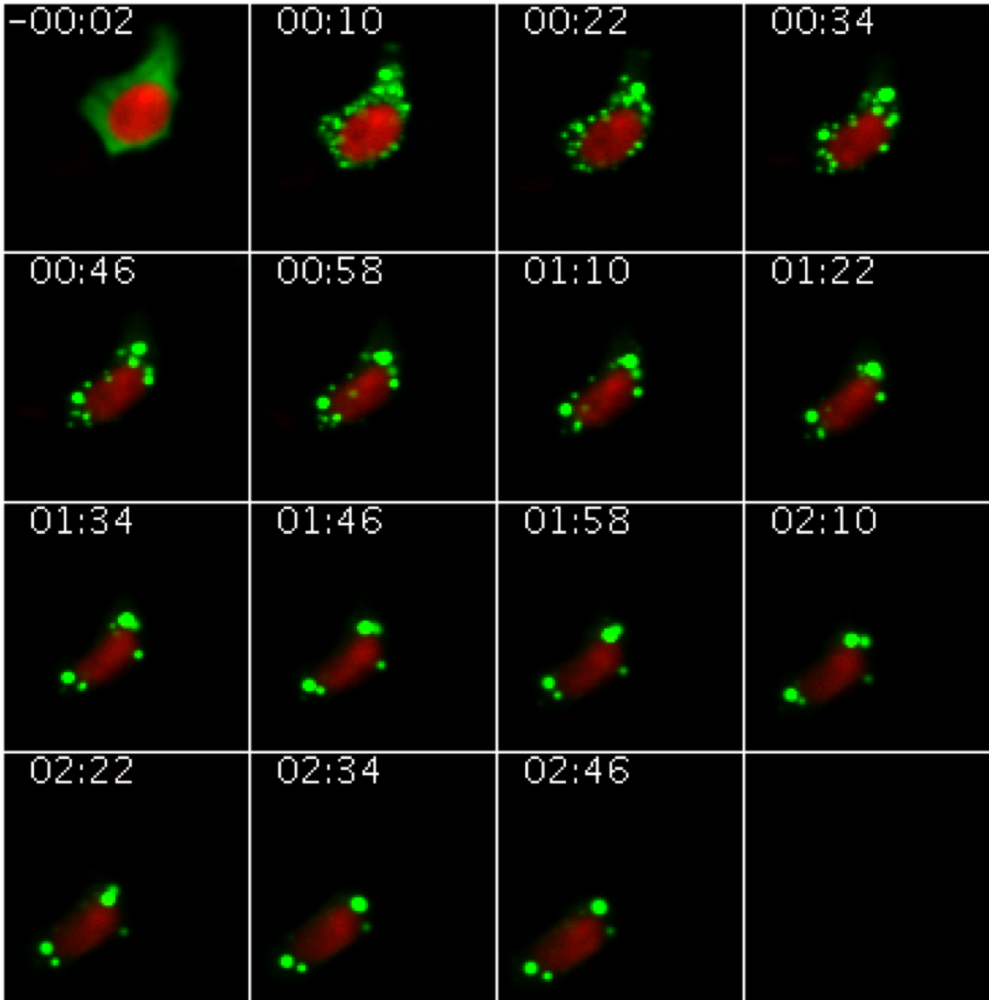


**Figure S5. Time-lapse fluorescence images of the cell expressing PKA-SPARK upon addition of isoprenaline, Related to Figure 3**. Time is shown in hour:minute. See also Movie S3.

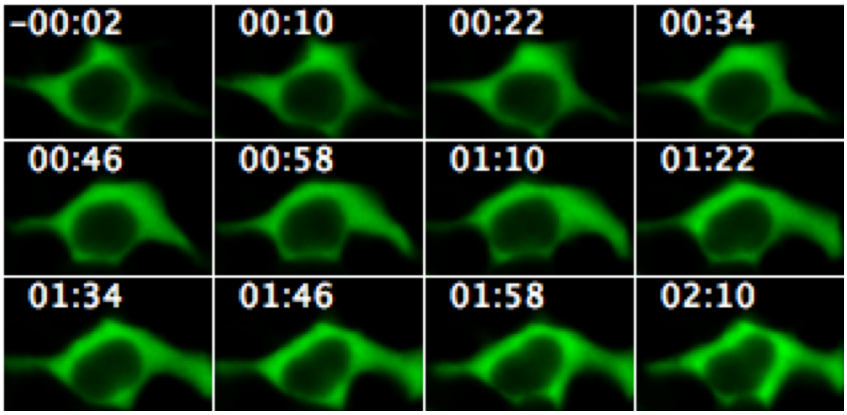


**Figure S6. Time-lapse fluorescence images of the PKA-SPARK expressing cell pre-incubated with carvedilol upon addition of isoprenaline, Related to Figure 3**. Time is shown in hour:minute.

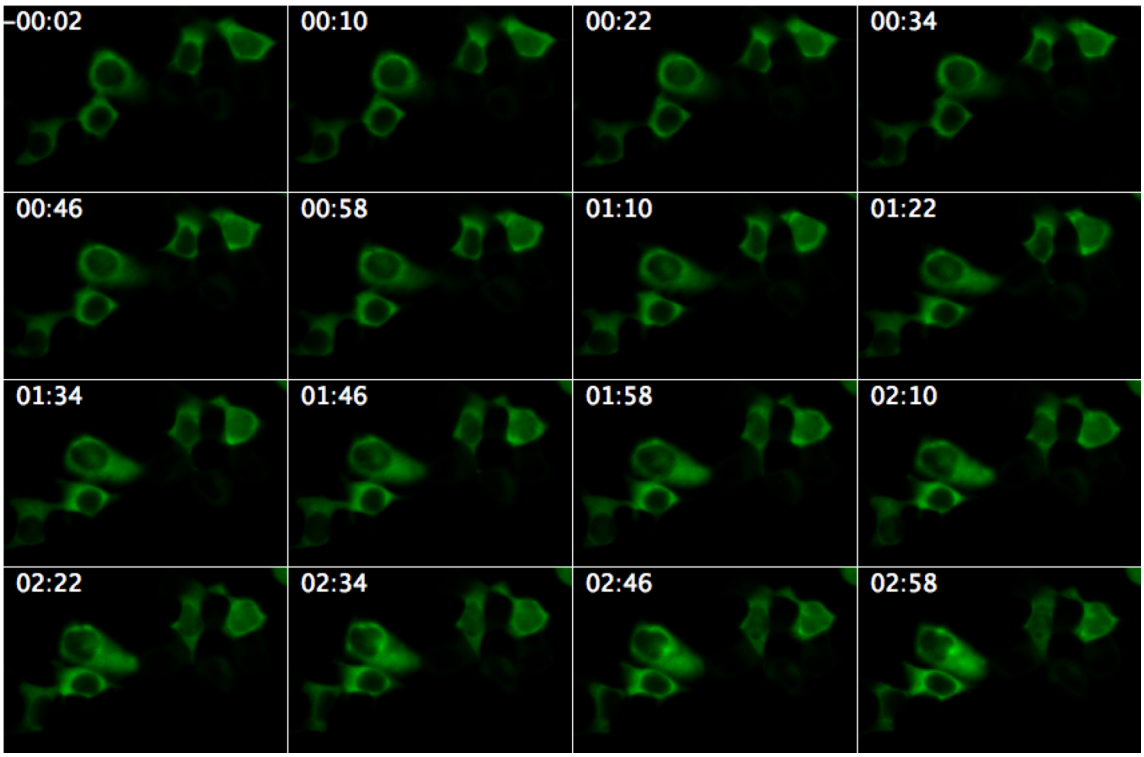


**Figure S7. Time-lapse fluorescence images of HEK293 cells expressing PKA-SPARK pre-incubated with caffeine upon addition of adenosine, Related to Figure 3**. Time is shown in hour:minute.

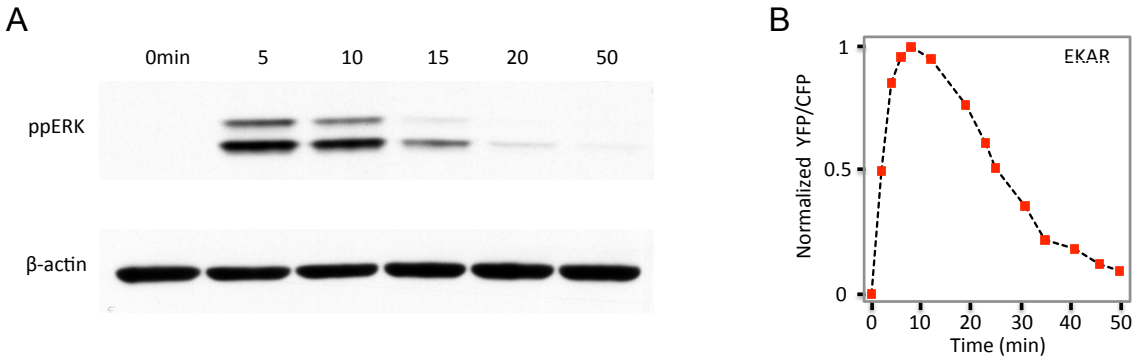


**Figure S8. Characterization of ERK activation upon EGF stimulation, Related to Figure 4**. (A). Western blot of ppERK upon EGF stimulation of HEK293 cells, with b-actin as a loading control. (B). Time-dependent fluorescence ratio change of the FRET ERK reporter EKAR upon addition of EGF in HEK293 cells. The normalized ratio of yellow fluorescence of YFP (yellow fluorescent protein) over cyan fluorescence of CFP (cyan fluorescent protein) was plotted against time.

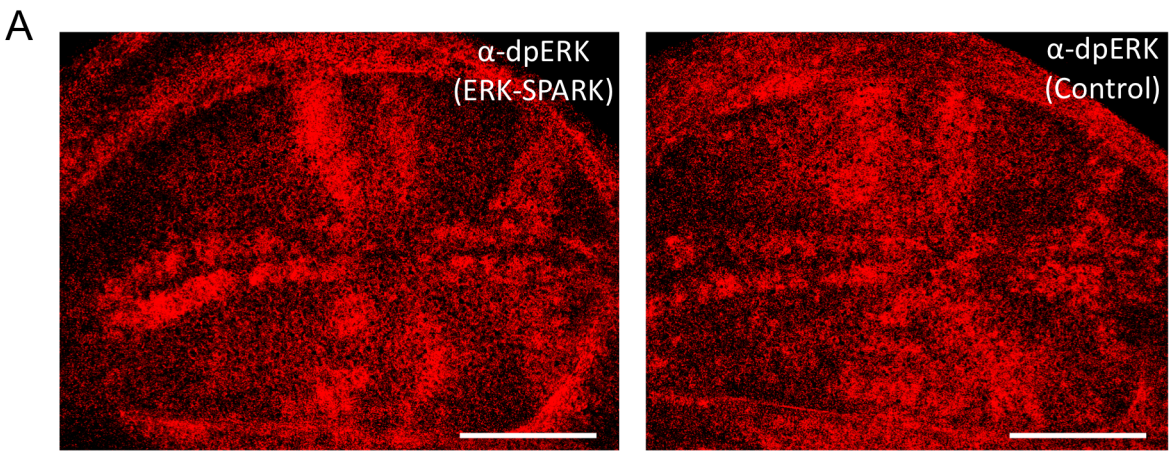
A
α-dpERK
(ERK-SPARK)
α-dpERK
(Control)

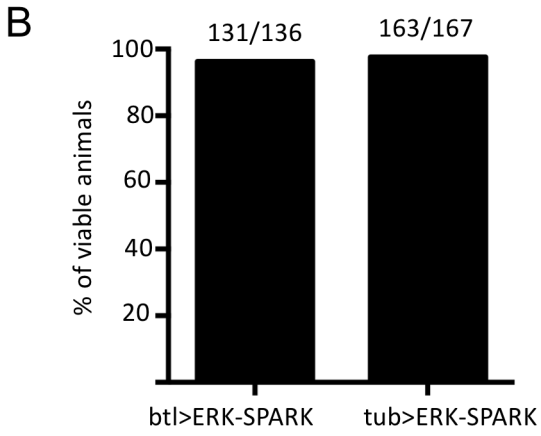
B
131/136
163/167
100
80
60
40
20
% of viable animals
btl>ERK-SPARK
tub>ERK-SPARK

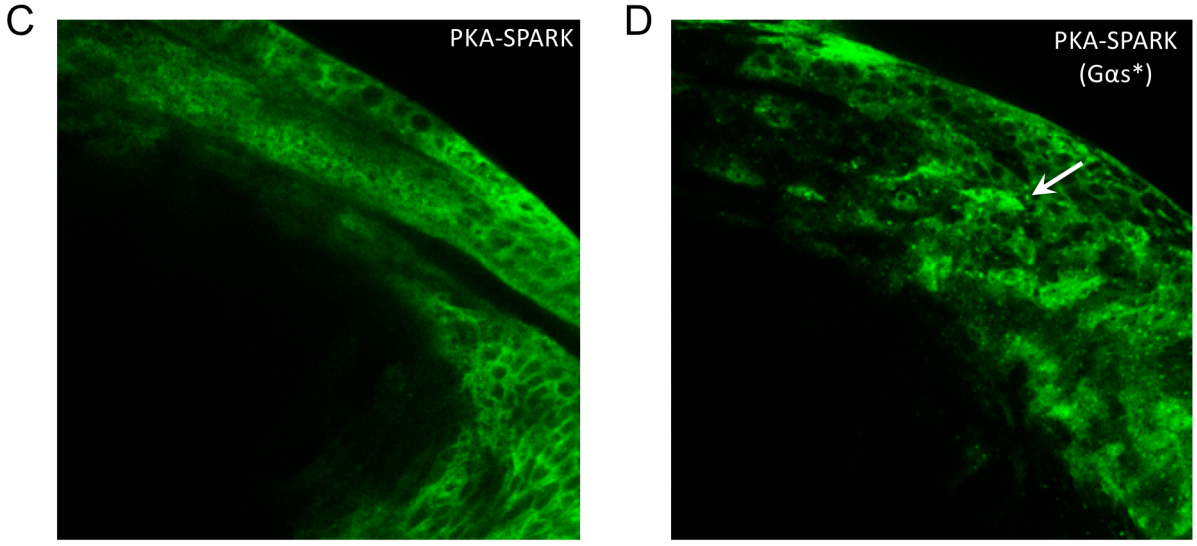
C
PKA-SPARK
D
PKA-SPARK
(Gαs*)

**Figure S9. Characterization of SPARK in Drosophila.** (A) Antibody staining of dpERK in the wing disc in *Drosophila*, Related to Figure 5. Left, dpERK staining of a wing disc expressing ERK-SPARK. Right, dpERK staining of a control wing disc. (B) Viability of Drosophila expressing ERK-SPARK, Related to Figure 5. ERK-SPARK was expressed in trachea (btl>ERK-SPARK), or ubiquitously in whole animals (tub>ERK-SPARK). The bar graph represents the number of flies expressing Erk-SPARK over their siblings that possessed balancers. The ratio of animals expressing Erk-SPARK in the trachea (btl-Gal4/+; UAS-Erk-SPARK/+) versus control siblings (btl-Gal4/+; +/TM6B) is 131/136. The ratio of animals ubiquitously expressing Erk-SPARK (tub-Gal4/Erk-HT) versus control siblings (Erk-SPARK/TM3) is 163/167. The survival ratios respect Mendelian distribution. (C) Fluorescence images of PKA-SPARK expressing cells in the wing imaginal disc in Drosophila, Related to Figure 5. (A) Wild type wing imaginal disc. (B) Wing imaginal disc expressing a constitutively active form of a G protein (Gαs*).

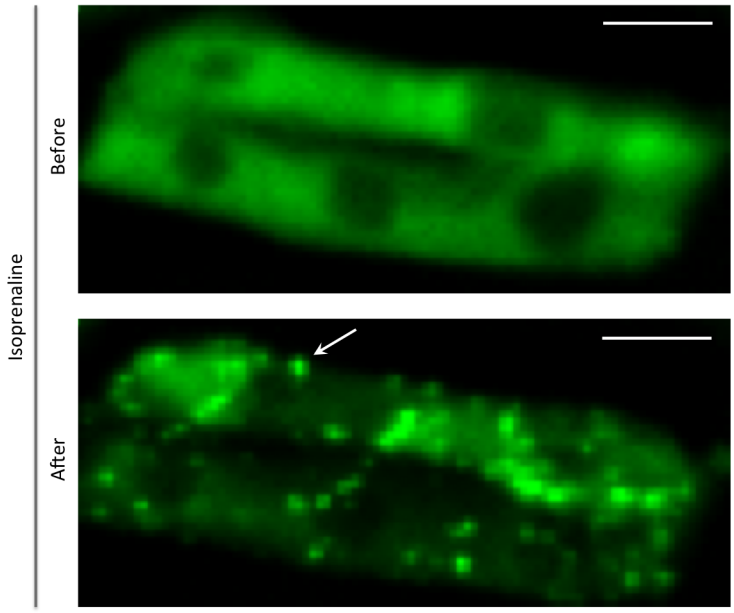


**Figure S10. Demonstration of PKA-SPARK in zebrafish, Related to Figure 5**. The plasmid encoding PKA-SPARK was injected into zebrafish embryo. The skeletal muscle cells were imaged in the live embryo before and 30 minutes after addition of isoprenaline. Arrow points to EGFP droplet. Scale bar, 10 μm.